THE COINCIDENCE OF NUCLEAR STAR CLUSTERS AND ACTIVE GALACTIC NUCLEI

Anil Seth[*]
Harvard-Smithsonian Center for Astrophysics

Marcel Agüeros[†]
Columbia University

Duane Lee
Columbia University

Antara Basu-Zych
Columbia University
Accepted by ApJ, Dec. 20, 2007

ABSTRACT

We study galaxies that host both nuclear star clusters and active galactic nuclei (AGN) implying the presence of a massive black hole. We select a sample of 176 galaxies with previously detected nuclear star clusters that range from ellipticals to late-type spirals. We search for AGN in this sample using optical spectroscopy and archival radio and X-ray data. We find galaxies of all Hubble types and with a wide range of masses ($10^9 - 10^{11}$ M$_\odot$) hosting both AGN and nuclear star clusters. From the optical spectra, we classify 10% of the galaxies as AGN and an additional 15% as composite, indicating a mix of AGN and star-formation spectra. The fraction of nucleated galaxies with AGN increases strongly as a function of galaxy and nuclear star cluster mass. For galaxies with both a NC and a black hole, we find that the masses of these two objects are quite similar. However, non-detections of black holes in Local Group nuclear star clusters show that not all clusters host black holes of similar masses. We discuss the implications of our results for the formation of nuclear star clusters and massive black holes.

Subject headings: galaxies:nuclei – galaxies: active – galaxies:star clusters – galaxies:formation

1. INTRODUCTION

Nuclear star clusters (NCs) are massive star clusters coincident with the photocenters of galaxies. They are very common and have been found in ~75% of local late-type spirals (Böker et al. 2002) and Virgo dwarf elliptical galaxies (Côté et al. 2006). Their size is similar to that of globular clusters (Böker et al. 2004), but NCs are 1-2 orders of magnitude brighter and more massive (Walcher et al. 2005). Also, unlike most globular clusters, they have extended star formation histories (Walcher et al. 2006; Rossa et al. 2006) and complex morphologies (Seth et al. 2006).

The luminosity of nuclear star clusters correlates with galaxy luminosity in both ellipticals (Lotz et al. 2001; Graham & Guzmán 2003; Côté et al. 2006) and spirals (Carollo et al. 1998; Böker et al. 2004). Recently, it has been shown that the masses of NCs follow scaling relationships with galaxy mass (M_{gal}), bulge velocity dispersion (σ), and Sérsic index (Ferrarese et al. 2006; Wehner & Harris 2006; Rossa et al. 2006; Graham & Driver 2007). These scaling relations are very similar to those seen for massive black holes (MBHs[1]), appearing to extend those relations

[*]CfA Fellow
Electronic address: aseth@cfa.harvard.edu
[†]NSF Astronomy and Astrophysics Postdoctoral Fellow
[1] We use massive black holes to refer to all non-stellar-mass black holes, including those normally referred to as intermediate

to lower masses. Thus, Wehner & Harris (2006) and Ferrarese et al. (2006) suggest that there may be a single scaling relation linking the mass of a central massive object (CMO; either a NC or MBH) to the large-scale properties of the galaxy. The existence of an $M_{CMO} - \sigma$ or $M_{CMO} - M_{gal}$ relation suggests that the formation of the CMO is linked in some way to the evolution of the galaxy. Theoretically, these scaling relationships can be understood in multiple ways. They could be created by feedback from either NCs or MBHs regulating the star formation in the galaxy as a whole (e.g., McLaughlin et al. 2006b), or alternatively, they could simply result from gas accretion onto the nucleus in proportion to the galaxies' mass (e.g., Li et al. 2007).

Despite this interesting connection between NCs and MBHs, and their link to galaxy formation and evolution, no systematic study of the overlap between these classes of objects exists. A handful of objects, including the Milky Way, are already known to host both NCs and MBHs (see §4). Ferrarese et al. (2006) and Wehner & Harris (2006) show there is a rough transition at galaxy masses of ~10^{10} M$_\odot$ (and corresponding CMO mass of ~10^7 M$_\odot$), above which galaxies typically host MBHs, and below which galaxies have NCs. While there is good evidence that more massive galaxies do not in fact host NCs (Côté et al. 2006), it remains unclear how common MBHs are in lower mass galaxies (e.g., Greene & Ho

mass and as super-massive black holes.

2007). Recent theoretical work shows that MBHs could form from stellar mergers in a young, dense cluster environment (Miller & Colbert 2004; Portegies Zwart et al. 2004), and a direct link between NC and MBH formation may therefore exist.

We present a systematic study of the overlap between NCs and MBHs aimed at better understanding the relation between the two types of objects and the formation mechanism of CMOs in general. Starting with a sample of galaxies with known NCs, we search for active galactic nuclei (AGN) that are powered by accretion onto an MBH. This study gives a lower limit on the number of systems with MBHs, since quiescent and heavily obscured MBHs will not be detected as AGN.

We begin by describing our sample of galaxies with NCs, drawn from several different catalogs (§2). Using optical spectra and radio and X-ray data, we examine our sample galaxies for evidence of AGN activity (§3). We then review galaxies for which detections of both AGN or MBHs and NCs exist in the literature (§4). We discuss the demographics of galaxies with AGN and NCs, the relative masses of these CMOs in galaxies where they co-exist, and the implications of this study for CMO formation, in §5. We conclude and discuss future work in §6.

2. SAMPLE SELECTION & PROPERTIES

We have used catalogs from multiple studies to create a sample of nearby galaxies with known NCs. This sample, which contains galaxies of all Hubble types, is the starting point for finding galaxies that contain both NCs and MBHs.

The Hubble Space Telescope (HST) has enabled NCs to be identified in a large numbers of nearby galaxies with distances $\lesssim 30$ Mpc. The use of HST is important both for distinguishing the NCs amidst the crowded inner regions of galaxies and for resolving the clusters. In the studies used in our sample, the NCs have been selected from broadband optical or NIR images, and are seen as compact sources distinct from the underlying galaxy profile. In the vast majority of the selected galaxies, the NCs have been resolved, suggesting that they are stellar sources and not AGN emission (see discussion in Rossa et al. 2006). Spectral studies of a number of the NCs in our sample confirm that their optical spectrum is dominated by starlight (Walcher et al. 2006; Rossa et al. 2006).

We use the following catalogs of galaxies with nuclear star clusters:

1. Elliptical and lenticular galaxies from the ACS Virgo Cluster Survey of Côté et al. (2006). This survey includes both giant and dwarf elliptical galaxies in Virgo. Of the 100 elliptical galaxies in the survey, 51 contain NCs with measured properties (type "Ia" nuclei in Table 1 of Côté et al. 2006). These galaxies are all fainter than $M_B \gtrsim -19$; some brighter galaxies have apparent NCs but Côté et al. (2006) are unable to derive their properties. The brightest galaxies in their sample ($M_B < -20.5$) do not have any NCs. Of the 51 NCs, five are unresolved (see Table 5).

2. Early-type spiral galaxies from Carollo et al. (1997, 1998, 2002). Targets for their WFPC2 and NIC-

MOS snapshot programs are Sa-Sbc galaxies with $v_{hel} < 2500$ km/sec, angular diameter > 1', and an inclination $< 75°$. Combining their WFPC2 and NICMOS studies, there are a total of 58 out of 94 galaxies with NCs; these are resolved in all but two cases.

3. Late-type spiral galaxies from Böker et al. (2002). This sample includes bulgeless spiral galaxies of type Scd-Sm, with $v_{hel} < 2000$ km/sec and inclinations of $\lesssim 30°$. Of 73 galaxies, 59 were found to have NCs.

4. Edge-on late-type (Sbc-Scd) galaxies from Seth et al. (2006). Of the 14 galaxies in this sample, 9 have NCs, 6 of which are well resolved.

Our sample includes 176 galaxies with nuclear star clusters spanning all galaxy types. Although the galaxy samples used are not complete, none of the selection criteria for these samples depends on the nuclear properties of the galaxies.

Galaxy distances were determined from a variety of sources, including using Virgo-infall corrected velocities from Hyperleda (Paturel et al. 2003) and NED1D[2] for other distance indicators. For the Virgo cluster galaxies, a distance of 16.5 Mpc was assumed (Tonry et al. 2001; Mei et al. 2007). The galaxies range in distance between 2 and 40 Mpc, with most having distances between 10 and 30 Mpc. Galaxy magnitudes and Hubble types (including numerical types, "T") were also determined from Hyperleda. Figure 1 shows the type and absolute magnitude of all 176 galaxies in our sample. The B-band absolute magnitudes of these galaxies range between -15 and -21. Galaxy masses were obtained using galaxy colors to estimate the M/L ratios from Bell et al. (2003). We obtained optical color estimates for 147 of the 176 galaxies from Hyperleda (Paturel et al. 2003), including their B-V colors, as well as colors from the Sloan Digital Sky Survey (SDSS; York et al. 2000) and 6dF survey (Jones et al. 2004). To obtain masses we used both the Hyperleda total B magnitudes corrected for internal and foreground extinction (also obtained from Hyperleda), and where available, K band magnitudes from 2MASS and DENIS. In cases where multiple sets of photometric data were available, the median value for the galaxy mass was used. The masses determined for a single galaxy using different methods typically differ by ∼35% (0.15 dex). The sample galaxy properties and distances are given in Table 5.

2.1. Nuclear star cluster masses

The NCs in our sample have magnitudes measured in many different bands. To compare the NC properties for the entire sample we therefore estimated the mass for each NC. There is strong evidence that NCs, at least in spiral galaxies, have complicated star-formation histories (Walcher et al. 2006; Rossa et al. 2006; Seth et al. 2006). Therefore, derivation of NC masses from integrated magnitudes is not straightforward. We have estimated the masses for the NCs in our sample using a variety of methods, as detailed below. The derived masses are shown in Table 5 and are used in determining the relative masses

---

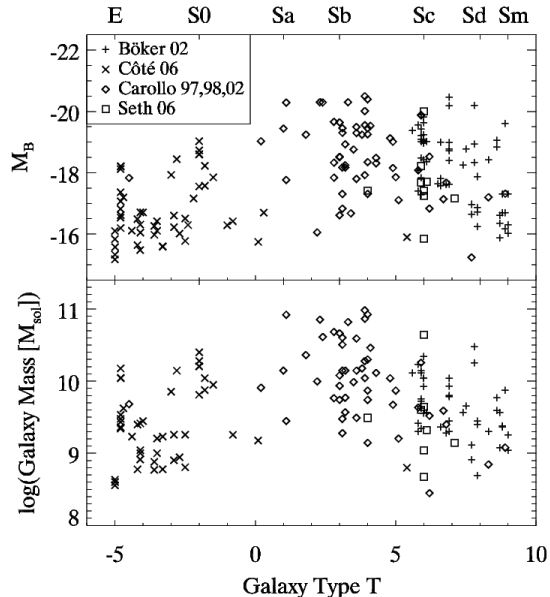[2] http://nedwww.ipac.caltech.edu/level5/NED1D/

Fig. 1.— *Top* – The galaxy type and absolute magnitude of all 176 of our sample galaxies with known nuclear star clusters. The x-axis gives the numerical galaxy type "T" and corresponding Hubble type from Hyperleda (Paturel et al. 2003). Symbols indicate the source catalog for each galaxy as discussed in the text. *Bottom* – The galaxy mass for all 147 galaxies for which colors were available from Hyperleda.
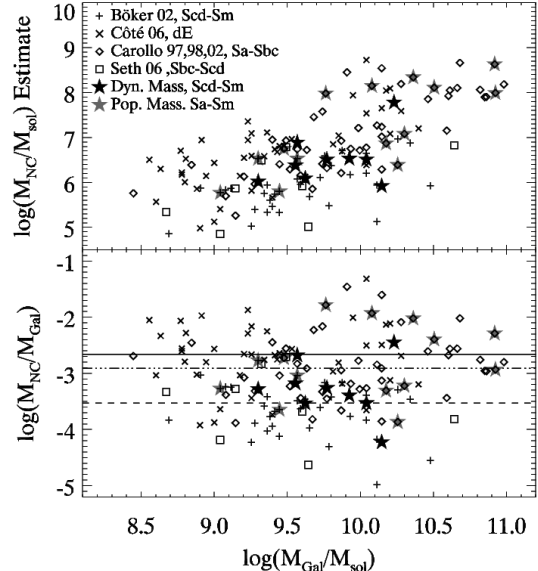

Fig. 2.— *Top* – Nuclear star clusters mass vs. galaxy mass for all the clusters with derived galaxy masses in our sample. *Bottom* – ratio of nuclear star cluster mass to galaxy mass. Overplotted are the median ratios for the elliptical galaxies (solid line), the early type spirals (dot-dashed line) and the late-type spirals (dashed-line). In both panels the stars indicate dynamical masses measured for late-type spirals by Walcher et al. (2005) (black stars), and the spectral synthesis masses from Rossa et al. (2006) (gray stars).

of NCs and MBHs and for examining the demographics of galaxies hosting both types of objects (see §5).

1. The best available mass estimates are dynamical measurements of 9 NCs in the Böker sample by Walcher et al. (2005) and masses from population synthesis fits for an additional 15 spiral galaxies in Rossa et al. (2006).

2. For the Côté et al. (2006) clusters, we followed the prescription of Ferrarese et al. (2006), who estimate the NC mass by assuming an age of 5 Gyr and use the cluster's published $g - z$ color to determine the metallicity and thus the appropriate mass-to-light (M/L) ratio from Bruzual & Charlot (2003).

3. For the early type spiral galaxies in the Carollo sample, we use the mean B-band M/L ratio of 3.64 ± 1.03 derived for early type spiral NCs by Rossa et al. (2006). For most of the galaxies, both V (WFPC2-F606W) and H (NICMOS-F160) magnitudes are available for each cluster, while a minority of galaxies have just one or the other magnitude available. We derive B-band magnitudes by assuming the colors of an SSP with Z = 0.030 (matching the derived mean metallicity in Rossa et al. 2006) and age of 5.9 Gyr to match the B-band M/L ratio (Bruzual & Charlot 2003). These magnitudes were corrected for the foreground and estimated internal extinction as determined from Hyperleda (Paturel et al. 2003), the mean extinction correction was $A_V = 0.27$.

4. For the late-type spiral galaxies, Walcher et al. (2005) has shown that the typical I-band M/L ratio is 0.50 ± 0.37. We used this to derive masses from

the I-band magnitudes in Böker et al. (2002) and Seth et al. (2006), after correcting for foreground and internal extinction. We note the possibility that because of the selection of objects with bright apparent magnitudes, the Walcher et al. (2005) spectroscopic sample may not be representative of the Böker et al. (2002) sample as a whole. This may result in an underestimate of the M/L ratio, as the study would favor younger, brighter NCs.

For the NCs with available dynamical masses (Walcher et al. 2005) or stellar population model masses (Rossa et al. 2006), the agreement between these masses and those obtained using the methods outlined above is good, with a mean difference of -0.02 ± 0.34 dex. This standard deviation of 0.34 dex (factor of ~ 2) gives some indication of the error in our NC mass determinations.

Figure 2 shows the derived NC masses as a function of galaxy mass. Although correlations between NC and galaxy luminosities or masses have been shown for samples of galaxies of a single type (Carollo et al. 1998; Böker et al. 2004; Côté et al. 2006; Rossa et al. 2006; Ferrarese et al. 2006; Wehner & Harris 2006), this is the first time they have been compared across all Hubble types. Figure 2 shows the expected correlation between NC mass and galaxy mass. However, we find an offset between earlier- and later-type galaxies, with the later-type galaxies having less massive NCs at a given galaxy mass. This can be seen in the bottom panel of Figure 2, where we plot the ratio of NC to galaxy mass. Lines indicating the median NC to galaxy mass ratio for elliptical, early type spiral, and late-type spiral galaxies show that late-type spirals have NC masses about an order of magnitude below elliptical galaxies of the same mass. We will discuss these results in greater detail in a future paper.

3. PRESENCE OF AGN

In this section we analyze the evidence for active galactic nuclei (AGN) in our sample galaxies using optical spectroscopy (§3.1) and radio and X-ray data (§3.2). We then examine the strength of the evidence for these detections being massive black holes in §3.3.

3.1. *Emission-line spectroscopy*

Of the 176 galaxies in our sample, 70 had possible nuclear spectra available in the SDSS Data Release 6 (DR6) (Adelman-McCarthy et al. 2007). After visually inspecting the location of each spectrum, we found that 62 spectra were coincident with the galaxy nuclei. Emission line fluxes determined after modelling of the underlying stellar populations were kindly provided by C. Tremonti (*private communication*) using the method described in Tremonti et al. (2004), and available for SDSS Data Release 4 (DR4) data at http://www.mpa-garching.mpg.de/SDSS/DR4/. The DR6 spectra used differ somewhat from earlier spectra. Most notably, the spectrophotometric zeropoint has changed, increasing fluxes by $\sim 35\%$ but leaving line ratios unchanged. In general, the line ratios from the DR6 spectra agree very well with those in DR4. The formal errors on the line fluxes were scaled by factors of $1.4 - 2.5$ (depending on the line) to include errors in the continuum subtraction and flux calibration derived from sources with multiple spectra as described on the Garching DR4 website[3]. These errors were then propagated to the line ratios. We select emission line galaxies in the SDSS spectrum by requiring that three of four strong lines (Hβ, [OIII] λ5007, Hα, and [NII] λ6584) have detections above 3σ. Of the 62 spectra in the sample, 25 meet this criterion.

We also find 23 galaxies that were observed as part of the Palomar Survey (Filippenko & Sargent 1985), 20 of which have detected emission lines (Ho et al. 1997a, hereafter HFS97[4]). As with the SDSS data used above, the emission line measurements are made after subtraction of the underlying stellar population based on spectral modelling. Errors in the line ratios were estimated using the data quality flags and assuming a conservative baseline uncertainty of 30%, with 50% and 100% uncertainties for sources with uncertainty flags of 'b' and 'c' respectively. Ten of these galaxies overlap with the SDSS spectra, giving a total of 75 galaxies for which we have nuclear spectra.

Of the 75 galaxies for which we have nuclear spectra, 39 have weak or undetected emission lines; we classify these galaxies as having absorption-dominated spectra. For the remaining 36 emission-line spectra, we followed the classification scheme of Kewley et al. (2006) to separate the sample into star-forming galaxies, composite objects, or Seyfert and LINER AGN. This classification scheme relies on four line ratios, [OIII]/Hβ, [OI]/Hα, [NII]/Hα, and [SII]/Hα.

Three emission line ratio diagrams (BPT diagrams; Baldwin et al. 1981) are shown in Figure 3. This figure shows line ratios from the full DR4 sample of galaxies in grayscale contours and small black points along with our

sample galaxies as red (SDSS) and blue (HFS97) dots. The green lines indicate the demarcation lines used in the classification scheme (Kewley et al. 2006). The primary classification of galaxies into star-forming, composite objects, or AGN is done using the [NII]/Hα vs. [OIII]/Hβ diagram (left panel of Figure 3)[5]. Spectra are classified as being AGN if they fall in the upper right part of the diagram above the theoretical maximum starburst line of Kewley et al. (2001) in the [NII]/Hα vs. [OIII]/Hβ diagram. Composite objects have emission lines thought to be caused by a mix of AGN and star-forming lines, and have line ratios falling below the Kewley et al. (2001) line and above the empirical Kauffmann et al. (2003) line. Galaxies below the Kauffmann et al. (2003) line have line ratios dominated by star formation. Further separation of AGN into LINER and Seyfert galaxies is done using the [SII]/Hα vs. [OIII]/Hβ and [OI]/Hα vs. [OIII]/Hβ diagrams (right two panels of Figure 3), with Seyferts lying at higher values of [OIII]/Hβ.

Using the [NII]/Hα vs. [OIII]/Hβ diagram, we classify 18 galaxies as having star-forming ("HII") spectra, 11 as having composite spectra ("C"), and 7 as having AGN-like spectra ("AGN"). The other line ratio diagrams suggest that 3 of the AGN are Seyferts ("S2") and 4 are LINERS ("L2"), while an additional 3 composite galaxies are also found to have LINER-like line ratios. For the ten overlapping galaxies (connected by orange lines in Figure 3), the classifications between the HFS97 and SDSS data agree in all cases, except for NGC 5879. This galaxy is classified as an AGN from both spectra, but is found to be a LINER only from the SDSS spectrum.

Our classifications also agree well with the somewhat different classification system used by HFS97 for the Palomar galaxies[6]. Eleven of the eighteen sources we classified as composite or AGN are in the HFS97 sample. Of these, 8 are classified as transition or AGN by HFS97. Specifically, the five galaxies that we classify as LINER and Seyfert AGN match their classifications exactly, while for the six galaxies we classified as composite, half of them were classified as star-forming, with the other half being LINERS or transition objects in their classification scheme. Both the composite class from Kewley et al. (2006) and the transition class from HFS97 are thought to result from a mix of star-forming and AGN spectra, thus a correspondence between these classes is expected. In the HFS97 classification the transition objects are objects with a mix of LINER and star-forming spectra, while in our classification they can be a mix of LINER or Seyfert and star-forming spectra.

One of the galaxies in the HFS97 sample, NGC 4750, was found to have broad Hα emission, and is thus classified by them as a L1.9. We have adopted this classification. Also, Shields et al. (2008) has recently found broad [NII] (but not Hα) emission lines in the composite galaxy NGC 1042. Visual inspection of the model-subtracted SDSS spectra suggest that none has any obvious broad

---

[3] http://www.mpa-garching.mpg.de/SDSS/DR4/raw_data.html
[4] We use the emission line measurements from HFS97, but not their spectral classifications.

[5] Due to the proximity of the emission lines used in these ratios, the [NII]/Hα vs. [OIII]/Hβ diagram is remarkably insensitive to reddening: 5 magnitudes of reddening creates a change of 0.006 and 0.08 dex in the [NII]/Hα and [OIII]/Hβ ratios respectively.
[6] The HFS97 classification system gives a primary role to the [OI]/Hα line ratio, which is quite weak in many of our spectra and significantly more susceptible to reddening than the [NII]/Hα ratio.
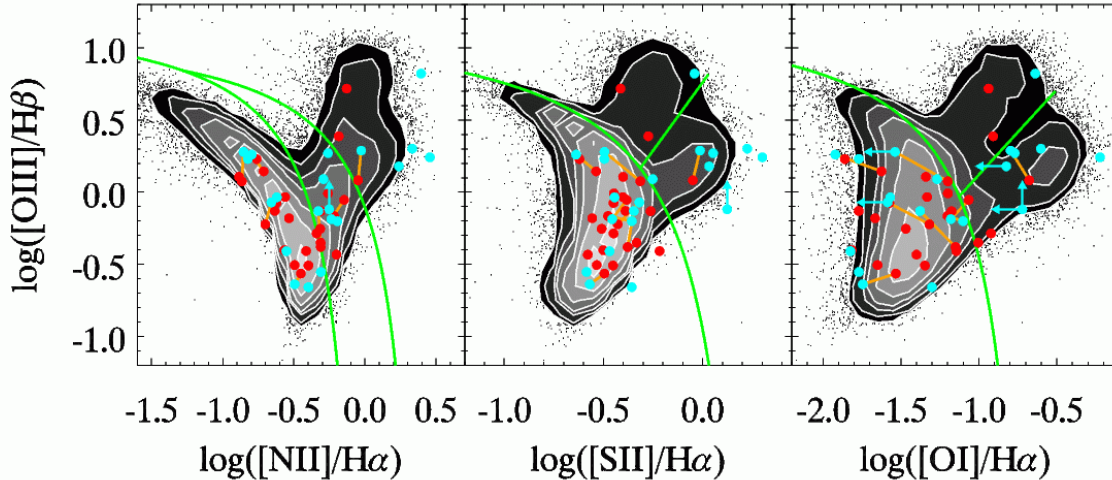
FIG. 3.— Emission line diagrams for galaxies in our sample. Red points show line ratios derived from SDSS DR6 data, blue are from Ho et al. (1997a); orange lines connect galaxies with both types of spectra. Grayscale and small black points indicate the Garching reduction of the full SDSS DR4 sample. Green lines indicate the classification system adopted from Kewley et al. (2006).

emission lines.

The line ratios used in our classification are given in Table 1 for the star-forming galaxies and in Table 2 for the composite and AGN galaxies (C/AGN). For the star-forming nuclei, Table 1 also gives the star-formation rates based on Hα luminosities derived from the relation given in Kennicutt (1998). Table 2 gives the [OIII] luminosities for the C/AGN nuclei which are used in §5.2. These line luminosities have been corrected for reddening assuming Hα/Hβ=2.85 for the star-forming galaxies and Hα/Hβ=3.1 for the C/AGN galaxies (Osterbrock 1989; Kewley et al. 2006).

To get a sense of the uncertainty in our classification, we repeated the classification after both adding and subtracting the 1σ errors to the [NII]/Hα and [OIII]/Hβ ratios. This changes the classification for a handful of galaxies: the number of composite galaxies varies between 8 and 12, while the number of AGN varies between 6 and 8. Seven galaxies have error bars crossing the HII/C boundary: C-classified NGC 428, 3423, 4206, 4517, and 4625 and HII-classified NGC 2964 and VCC 1250. Two galaxies have error bars crossing the AGN/C boundary: C-classified galaxy VCC 1619 and AGN-classified NGC 4411B.

Although the galaxies in our sample are quite nearby, the physical resolution of the spectra (3" fibers for SDSS, 2" slit for HFS97) is still significantly larger than the typical cluster sizes. For a galaxy at the median distance of our sample (16.5 Mpc), the corresponding spatial resolution is ∼ 200 pc. This could lead to detection of star-formation not coincident with the nucleus (Shields et al. 2007), and might be expected to dilute weak AGN emission, therefore causing genuine AGN to be classified as composite objects.

In summary, from the 75 galaxies with available optical spectra, we find 18 that have composite or AGN spectra. We discuss the fraction of these galaxies that have MBHs in §3.3. We now discuss the radio and X-ray properties of our sample galaxies.

3.2. *Radio and X-ray correlations*

In order to explore the multiwavelength properties of the galaxies in our sample, we matched the NC positions to a number of radio and X-ray catalogs. While the cataloged observations at these wavelengths are unable to resolve structures on the sub-arcsecond scale of the NCs, detections in the radio and/or the X-ray regimes can be used to place limits on the emission from putative AGN independently of the information derived from optical spectra.

3.2.1. *Radio data*

Galaxies that are radio sources are thought to host either active star formation or AGN. Radio observation of AGN show they have compact nuclear radio sources with high brightness temperatures that cannot be reproduced by starbursts (e.g., Terashima & Wilson 2003). Such radio sources are detected in about a third of galaxies classified as composite or AGN objects in the Palomar survey (Nagar et al. 2005). Sources with $L_{1.4\ GHz} \geq 10^{23}$ W Hz^{-1} are generally called radio-loud AGN, and are unambiguous evidence of an AGN (Best 2004). However, these sources are typically associated with very massive galaxies, and thus it is unlikely we will find radio-loud AGN in our sample (Croft et al. 2007).

We used the Very Large Array (VLA) Faint Images of the Radio Sky at Twenty-Centimeters (FIRST; Becker et al. 1995) to search for radio counterparts to the galaxies in our sample. FIRST is the deepest large-scale radio survey currently available; the limiting flux density is about 1.0 mJy, the survey resolution is ∼ 5", and the footprint is roughly the same as that of SDSS. We queried FIRST for radio sources within 30" of our NCs and found 13 matches[7]. The median separation between the radio source and the cluster position is 3 ± 9" (see Table 3). Of the 13 matched galaxies, we have optical-based classifications for nine (see Table 3). One galaxy, NGC 5377, is classified as an AGN/L2, while three others are classified as composite objects in our analysis. The

[7] Matching to the National Radio Astronomy Observatory (NRAO) VLA Sky Survey (NVSS; Condon et al. 1998), which covers the sky north of $\delta = -40°$ and includes sources stronger than ∼ 2.5 mJy, returned a larger number of matches, 52, including all of the FIRST-detected objects. However, the resolution for NVSS is roughly 45" FWHM and the survey data are therefore far less useful for our purposes.
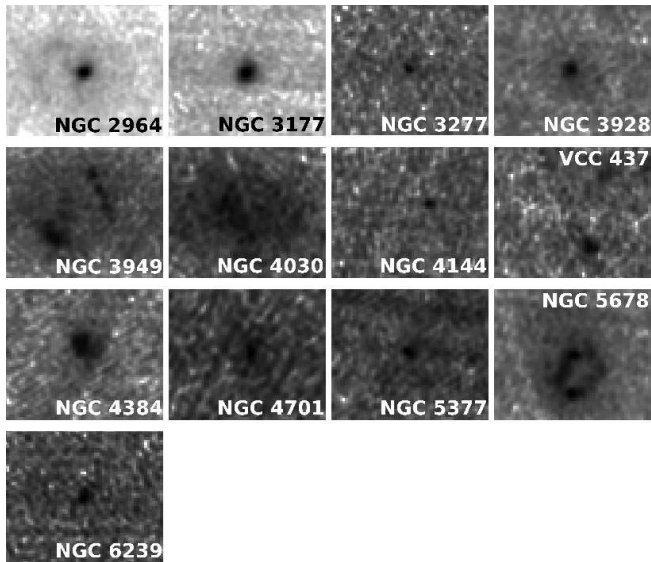
FIG. 4.— FIRST images of the 13 galaxies for which we find a catalog match within $30''$. Each image is roughly $1.6'$ in height and $2'$ in width and centered on the optical position of the nuclear star cluster in the galaxy.

remaining five galaxies have star-forming optical spectra. Unsurprisingly, the $L_{1.4GHz}$ for all these objects is well below 10^{23} W Hz^{-1}.

Visual inspection of the corresponding radio images did not find morphological evidence for the presence of an AGN (e.g., jets) in any of these (see Figure 4). In most cases, the radio emission appears diffuse, as expected if it is due to star formation. However, NGC 5377 and two of the three composite objects (NGC 3177 and NGC 3928) with radio detections appear as point sources in the FIRST images, consistent with the presence of a possible nuclear AGN source. For NGC 5377, higher resolution observations do confirm this source as an AGN (Nagar et al. 2005); similar radio observations are needed to determine the nature of the other sources.

An additional 94 galaxies from our sample fall within the FIRST footprint but do not have detections. White et al. (2007) have developed a method for obtaining the FIRST radio flux density for a group of sources when individual group members are undetected in the survey. Accordingly, we calculated a stacked image for our undetected sources. We applied the correction, prescribed in White et al. (2007), to account for the snapshot bias and derived our errors from the bootstrapping method (Efron 1982), which tests how individual entries affect the stacked average. We found that the average radio flux density for the undetected galaxies in the FIRST footprint is $\sim 90 \pm 20$ μJy (whereas the detected galaxies have flux densities of 1.6 to 68 mJy). This stacked "detection" provides an average measurement of the radio intensity for the typical nuclear region in these galaxies. At best, this suggests that any putative radio AGN in these galaxies is extremely weak. We note that among these non-detections are four galaxies we have classified as C/AGN objects using optical spectroscopy: NGC 4411B, VCC 1619, NGC 5806, and NGC 5879.

3.2.2. X-ray data

X-rays are one of the most direct evidences of nuclear activity and X-ray observations are therefore essential in

revealing the accretion processes taking place near the central black holes in AGN. With the spatial resolution of the new generation of X-ray telescopes, it is becoming possible to isolate low-luminosity AGN from other X-ray sources in a galaxy (e.g., Ho et al. 2001). In particular, the ability to detect photons with energies of several keV allows for the uncovering of AGN hidden at other wavelengths by column densities as high as $N_H \sim 10^{24}$ cm^{-2} (Ho et al. 2001).

We matched our sample to the combined *ROSAT* All-Sky Survey (RASS) Bright and Faint Source Catalogs (Voges et al. 1999, 2000). We also queried the High Energy Astrophysics Science Archive Research Center website for matches from the various catalogs of pointed *ROSAT* observations, *Chandra* sources, and *XMM-Newton* detections[8].

The X-ray data obtained in this fashion is rather heterogeneous, since the queried catalogs and instruments are very different in nature. For example, while none of the *Chandra* or *XMM* surveys covers as much sky as the RASS, the latter's positional accuracy is generally relatively poor (typically at least $15''$). In a similar vein, *Chandra* and *XMM* both have greater sensitivity than *ROSAT*, but the telescopes are not designed to detect sources in exactly the same energy ranges.

In order to produce the data for the matches listed in Table 4, we proceeded as follows:

1. Since *Chandra* typically has better positional accuracy than *XMM*, and both typically have better accuracy than *ROSAT*, we used *Chandra* data preferentially, then *XMM*, then *ROSAT*, in our analysis.

2. For galaxies with *Chandra* and/or *XMM* detections, there were frequently multiple X-ray sources. In those cases we chose the source closest to the optical position of the NC[9]. The median offset for the 13 *Chandra/XMM* sources is $1.3'' \pm 1.4''$, with the largest offset being $4.9''$. All the *Chandra* data come from XAssist (an automated extraction pipeline for X-ray data; Ptak & Griffiths 2003); these are the sources with an "X" prefix in Table 4. The *XMM* data are from the second catalog of the *XMM* serendipitous survey (2XMM sources; Watson et al., in prep.).

3. Of the 8 galaxies with RASS matches, half had detections in pointed catalogs, and we therefore used those data to characterize the X-ray sources. Three of the other galaxies, NGC 3259, NGC 4030, and NGC 4540, are published X-ray sources (identified as such by Véron-Cetty et al. 2004; Moran et al. 1996; Mickaelian et al. 2006). The positional offsets between the RASS source and the NC are small ($\leq 10''$) for the two first galaxies, and the associations with the RASS sources seem secure. However, NGC 4540 and NGC 2566 both have large positional uncertainties and offsets from the NCs.

[9] The positional accuracy of our NC positions is dominated by the uncertainty in the HST astrometry, which is typically accurate to within $1-2''$.

Pointed observations are clearly required to confirm that these two galaxies are X-ray sources, and we consider these associations to be tentative.

4. Four more galaxies are included in various *ROSAT* pointed surveys and/or identified as X-ray sources in the literature. Two of these are from catalogs of High Resolution Imager (HRI) sources (Panzera et al. 2003; ROSAT Scientific Team 2000)[10]. In both these galaxies, NGC 1385 and NGC 6000, the offset with the NC is less than the 5″ nominal positional accuracy for HRI observations (Flesch & Hardcastle 2004). The two other sources were detected with the other X-ray instrument aboard *ROSAT*, the Position Sensitive Proportional Counter (PSPC), whose positional accuracy is closer to 30″. Flesch & Hardcastle (2004) identify NGC 600 as a PSPC source with 61% confidence[11]; the offset between the X-ray source (positional uncertainty 13″) and the NC is 10″. White et al. (1996) include NGC 3445 in their WGACAT[12].

5. We used WebPIMMS (Mukai 1993) to calculate $2 - 10$ keV fluxes for all of these sources, assuming a canonical intrinsic power-law spectrum with photon index $\Gamma = 1.8$ (for low-luminosity AGN Γ ranges between 1.6 and 2.0; Terashima & Wilson 2003) absorbed to the Galactic value. We then calculate the X-ray luminosities given in column 7 of Table 4. These values are consistent with those in the literature for the known X-ray-emitting galaxies, once differences in the adopted distances and energy bands are taken into account.

A complicating factor in interpreting the X-ray luminosities we obtain at the end of this process is the differing point spread function (PSF) for each of these telescopes. While, broadly speaking, *Chandra*, *XMM*, and the HRI on *ROSAT* have similar PSFs (from ~ 1 to 6″), the *ROSAT* PSPC has a PSF with a $\sim 30″$ FWHM (Panzera et al. 2003), and the PSFs all vary with position on the detector and photon energy. Determining which sources are extended and which are truly point-like is therefore difficult, with the exception of the *Chandra* sources, for which XAssist provides sub-arcsecond measurements of source extent (listed in column 6 of Table 4). The situation with the 2XMM sources is relatively straightforward: any source that is smaller than the 6″ PSF and hence unresolved is set in the catalog to have a 0″ extent.

The RASS sources (PSPC detections) all have associated cataloged extent measurements and extent likelihoods (see Voges et al. 1999); however, these values should be treated with caution (e.g., for bright sources the deviations of the PSF from a Gaussian lead to incorrect extent measurements), and are considered reliable only if the extent measurement is $> 10″$ and the likelihood is > 10 (F. Haberl, *private communication*; see also Haberl et al. 2000). For three of the RASS sources the measured extent and extent likelihood are both 0″; for the fourth, RX J120023−01055 (NGC 4030), the cataloged extent is 9″, but the extent likelihood is 1, implying the source is actually unresolved.

For the sources with pointed *ROSAT* observational data, the definition of source extension varies from catalog to catalog. For the two sources detected by the HRI, 1BMW 033728.0−243003 and 1RXH J154949.7−292310 (counterparts to NGC 1385 and NGC 6000), the extents are given as 0″. However, Panzera et al. (2003) give the actual source extent for NGC 1385 as 14″ (with extent likelihood 0). The catalog entry for NGC 6000 indicates that it is not extended, but does not give an associated measurement. As for the PSPC sources, 2RXP J013305.7−071835 (NGC 600) is fit by a Gaussian with $\sigma = 12″$, and is given an extent likelihood of 0 in the PSPC catalog (ROSAT Scientific Team 2000). Finally, the WGACAT is defined as a point-source catalog, and no measurements are included in the available data.

In summary, we find a total of 22 X-ray sources associated with NCs in our sample. We evaluate how many of these may possess black holes in the following section.

3.3. *Do these sources harbor black holes?*

We now consider how reliably we can infer the presence of MBHs in the galaxies for which our multiwavelength data indicate the presence of AGN.

For the optical data, considerable work has been done to determine whether low-luminosity Seyferts, LINERS, and transition/composite objects do in fact represent MBH accretion. While Seyfert line ratios are a strong indicator of MBH accretion, it is not clear whether the same is true for all LINERs and transition/composite objects (see review by Ho 2004). Several recent studies of LINER galaxies suggest that a majority of them do in fact indicate the presence of an MBH based on high resolution radio observations (Nagar et al. 2005), X-ray emission (Dudik et al. 2005; González-Martín et al. 2006), and UV variability (Maoz et al. 2005). There are cases where LINER line ratios do seem to be produced by star formation. For instance, in the LINER galaxy M61 (NGC 4303), the recently formed stars provide more than enough ionizing flux to explain the observed Hα emission (Colina et al. 2002), suggesting that LINERS may sometimes just be caused by bursts of star formation. However, we note that in the context of our sample, a majority of the LINERS are found in early type spiral galaxies, whose NCs are known to only rarely host significant young stellar populations (Rossa et al. 2006). The nature of composite or transition objects, proposed to be a mix of AGN emission and star formation, is even more difficult to determine (Ho 2004). From a radio survey of the HFS97 catalog, Nagar et al. (2005) finds 16% of transition objects have compact radio detections, compared to ∼45% for the Seyferts and LINERs. The observation of broad-emission lines in NGC 1042 (which we classify as a composite object) by Shields et al. (2008) does provide strong evidence for a MBH in that galaxy. In summary, the presence of an AGN implies the presence of MBHs reliably in Seyferts and a majority of LINERS, but less reliably for sources with composite spectra.

---

[10] The Panzera et al. (2003) catalog is a re-analysis of the HRI observations with exposures longer than 100 s; the other catalog includes all HRI pointed observations.

[11] Flesch & Hardcastle (2004) use the ROSAT Scientific Team (2000) catalog of PSPC pointed observations as the basis for this match.

[12] White et al. (1996) generated their own point source catalog from all publicly available *ROSAT* PSPC observations.

For the radio data, the presence of AGN can only be safely inferred in cases where the emission is above a certain threshold. Below that threshold (typically $\sim 10^{23}$ W Hz^{-1}; Best 2004), either star-formation or low-level AGN can be responsible for the radio emission. The 13 galaxies with FIRST detections in our sample all have luminosities $< 10^{22}$ W Hz^{-1}, which is unsurprising given the low masses of galaxies in our sample and the observed correlation between galaxy mass and radio-loudness (Croft et al. 2007). We therefore cannot use L_R alone to identify radio AGN in our sample. While morphological information could distinguish between star-formation and AGN emission in galaxies with lower radio luminosities, the resolution of FIRST data is insufficient to place strong constraints on the nature of the sources in these galaxies. The radio data are therefore useful only in setting upper limits on any (low-level) emission from MBHs in these galaxies, which require higher resolution observations to be detected with confidence.

For the X-ray data, which provide insight into a larger fraction of the AGN bolometric flux than the narrow optical emission lines, any well localized source with $L_X \gtrsim 2 \times 10^{39}$ ergs/sec very likely originates from an MBH (e.g. van der Marel 2004). This criterion is met by only four of our sources, NGC 4750, NGC 6000, NGC 6951, and NGC 7418 (Table 4), two of which (NGC 4750 and NGC 6951) have available optical spectra and are classified as AGN. The other sources are either luminous but poorly resolved *ROSAT*/PSPC detections, or lower luminosity ($\sim 10^{38}$ ergs/sec) *Chandra* or *XMM* detections. For the *ROSAT*/PSPC detections, the resolution is quite poor (FWHM $\sim 30''$), and thus covers a significant portion of the galaxy (~ 3 kpc). The X-ray fluxes are within the range expected for normal galaxies (Shapley et al. 2001), and thus could originate either from collections of other X-ray sources or accretion onto an MBH (note we include the extended *ROSAT*/HRI source in NGC 1385 in this category as well). For the higher resolution *Chandra* and *XMM* observations, which are localized to be coincident with the NC (see Table 4), the sources with low X-ray luminosities overlap with those expected for X-ray binaries (Fabbiano 2006). For instance, luminous X-ray sources in the NCs of M33 and NGC 2403 are both thought to be X-ray binaries (Dubus et al. 2004; Yukita et al. 2007). Also, low-mass X-ray binaries (LMXBs) are commonly found in massive clusters; in a survey of globular clusters in Virgo, $\sim 25\%$ of the brightest globular clusters were found to have LMXBs (Sivakoff et al. 2007). The *Chandra* and *XMM* detections with $L_X \lesssim 10^{39}$ ergs/sec are therefore consistent with the presence of X-ray binaries in these NCs. However, many low-luminosity AGN appear to have X-ray fluxes in this luminosity range as well (e.g., Dudik et al. 2005; Panessa et al. 2006). In conclusion, the presence of an MBH powered source is strongly indicated for four X-ray sources, while for the remainder of the sources the X-ray energy could be resulting either from MBH accretion or from other X-ray sources.

Despite these uncertainties in identifying the presence of MBHs in single galaxies in our sample, the data presented here collectively provide good evidence that the overlap between NCs and MBHs is common. In total, 10 galaxies in our sample show strong evidence of an MBH, with ~ 30 more having some indication of a possible MBH. Furthermore, it is likely that many MBHs in our sample galaxies do not have enough activity to bring them to our attention; for example neither the central black hole of the Milky Way (Narayan et al. 1998; Shields et al. 2007) nor that of M32 (Ho et al. 2003), galaxies similar to those in our sample, would likely be detected as AGN in our study.

4. PREVIOUSLY KNOWN AGN/NC SOURCES

In this section we present galaxies previously known to host both a NC and an MBH or AGN. These can be added to our sample to explore the types of galaxies in which NCs and MBHs overlap. Furthermore, four galaxies presented below have measured black hole masses, enabling a comparison of their NC and MBH mass (§5.2).

We find nine galaxies previously identified as having both NCs and an AGN or MBH, three of which are contained in our sample. These are all galaxies in which the presence of both a NC and MBH/AGN is well substantiated (but see also Ghosh et al. 2006; Decarli et al. 2007).

The Milky Way hosts both a NC and an MBH. The NC in the Milky Way was first described by Becklin & Neugebauer (1968) using IR observations, and was found to have a FWHM of $3 - 5'$ (~ 10 pc), consistent with NCs in similar galaxies (Carollo et al. 2002). More recent studies using both star counts and kinematics show that the mass enclosed within the central 10 pc is $\sim 3 \times 10^7$ M$_\odot$ (Genzel et al. 1996; Schödel et al. 2007). The Galactic MBH has a mass of 3.7×10^6 M$_\odot$ (Ghez et al. 2005).

Another well known galaxy with a NC, AGN, and MBH is NGC 4395, an Sm type galaxy at a distance of 4.3 Mpc (Thim et al. 2004) with $M_B = -17.30$ (Paturel et al. 2003). The NC in NGC 4395 (Matthews et al. 1999) has an $M_I = -11.3$, an effective radius of $0.19''$ (3.9 pc), and a velocity dispersion of $< 30 \pm 5$ km/sec (Filippenko & Ho 2003). Based on the velocity dispersion, Filippenko & Ho (2003) suggest a mass for the NC of $\lesssim 6.2 \times 10^6$ M$_\odot$. Using the method described in §2.1 to derive NC masses in late-type galaxies, we estimate the NC mass to be 1.1×10^6 M$_\odot$. The AGN is one of the nearest and least luminous Seyfert 1 nuclei (Filippenko & Sargent 1989). The black hole has a measured mass of $3.6 \pm 1.1 \times 10^5$ M$_\odot$ (Peterson et al. 2005), roughly one-third the mass of the NC.

Graham & Driver (2007) note two elliptical/lenticular galaxies, NGC 3384 and 7457, which have measured black hole masses (Tremaine et al. 2002) and apparent nuclear star clusters. Although the nuclear sources in both cases are unresolved in HST observations presented by Ravindranath et al. (2001), both nuclear spectra are classified as absorption spectra by HFS97, suggesting they are in fact nuclear star clusters. Using distances from Jensen et al. (2003), we find the M_H of the NCs of -15.44 and -15.71 for NGC 3384 and 7457 respectively, corresponding to NC mass estimates of 2.1 and 2.7×10^7 M$_\odot$ (§2.1).

Four sources in Scarlata et al. (2004) appear to have compact nuclear star clusters and are classified as transition or AGN objects by HFS97. NGC 4321 (M100) and NGC 5921 are both Sbc galaxies with bright NCs ($M_R \sim -14$) classified as transition objects in HFS97. NGC 4321 is undetected at X-ray and radio wavelengths despite tar-
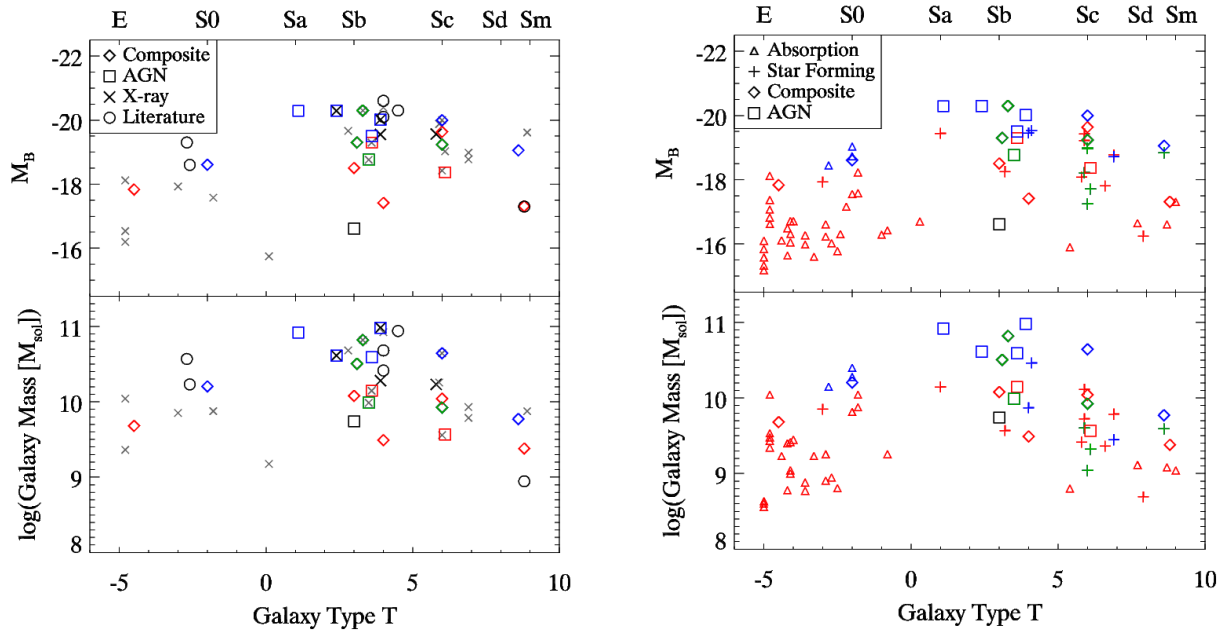
FIG. 5.— *Left* – The galaxy properties of all galaxies with NCs that also host candidate AGN. The red points indicate spectra from HFS97, blue points are SDSS spectra, and green points have both HFS97 and SDSS spectra. The four X-ray sources that are very likely AGN (see §3.3) are shown with large black X's, the rest of the detections have smaller gray X's. The six sources from the literature not contained within our sample are shown with circles (§4). The black square is ESO205-G7 (see §4, Rossa et al. 2006). *Right* – The galaxy type and absolute magnitude of all galaxies with spectra, colored as in the left panel. Note that because mass estimates are not available for all the galaxies (see §2), some data points in the top panel are missing in the bottom panel.

geted observations (Ho et al. 2001; Nagar et al. 2005). The two other galaxies (NGC 6384 and 6951) are in our sample and are classified as LINER and Seyfert respectively (§3.1). Also in our sample is the Sb galaxy ESO205-G7, mentioned in Rossa et al. (2006) as having a broad emission-line spectrum based on unpublished VLT/UVES spectra; however, this galaxy has no available spectrum or X-ray detection. Finally, the recent work by Gonzalez Delgado et al. (2007) analyzes HST WFPC2 archival data of AGN in the HFS97 survey, and includes observations of numerous objects that may host both NCs and AGN, including six of the galaxies for which we find overlap.

Possibly related to these galaxies are the recent detections of MBHs in the centers of two massive globular clusters thought to be the NCs of stripped dwarf galaxies (e.g., Meylan et al. 2001; Bedin et al. 2004). Dynamical observations of G1 and ωCen suggest they host black holes with masses $> 10^4$ M$_\odot$ (Gebhardt et al. 2002, 2005; Noyola et al. 2006; Rasio et al. 2006). In G1, this claim has been further strengthened by detection of X-ray and radio emission consistent with a 2×10^4 M$_\odot$ black hole (Pooley & Rappaport 2006; Ulvestad et al. 2007). There is also much more tentative evidence for MBHs in other globular clusters (Maccarone et al. 2007; Trenti 2006; McLaughlin et al. 2006a; van den Bosch et al. 2006).

In summary, we find six additional galaxies that have both NCs and MBHs, of which four have measured black hole masses.

5. DISCUSSION

We now discuss the most interesting results from our study. These include the demographics of galaxies with both AGN and NCs and the relative masses of MBHs and NCs. We also discuss our results in the context of models of the formation of NCs and MBHs.

5.1. *Demographics of galaxies with AGN & nuclear star clusters*

In this section we first discuss the range of properties spanned by the galaxies with both NCs and AGN, and then examine the detailed demographics of these galaxies in our spectroscopic sample.

The left panel of Figure 5 shows the Hubble type, mass, and absolute B-band magnitude of all galaxies presented in this paper hosting both NCs and candidate AGN, including sources from the literature (§4). Galaxies with both AGN and NCs cross all Hubble types and reach magnitudes as faint as $M_B \sim -16$ and galaxy masses as low as $\sim 10^9$ M$_\odot$. The AGN+NC galaxies are most common among early type spirals and brighter/more massive galaxies (e.g., Decarli et al. 2007). As discussed in §3.3, the sources most likely to be MBH+NC galaxies are the 7 spectroscopic AGN candidates (squares in Figure 5), the four brightest localized X-ray sources (black X's), and the six sources from the literature not contained within our sample (circles). Even these galaxies span a wide range of Hubble types and luminosities/masses. Thus the overlap of MBHs and NCs is a phenomenon that occurs in all types of galaxies between masses of 10^9 M$_\odot$ and 10^{11} M$_\odot$.

To be more quantitative about which galaxies host AGN and which do not, we limit ourselves to the 75 galaxies in the spectroscopic sample for which both the detections *and* non-detections of AGN are known. The right panel of Figure 5 shows the classification of all galaxies in the spectroscopic sample; triangles represent galaxies with absorption spectra, crosses the star-forming galaxies, diamonds the composite galaxies, and squares the AGN. Seven galaxies are classified as AGN (9% of the sample), and 18 as composite or AGN (24% of the sample). Based on our discussion in §3.3, this suggests that
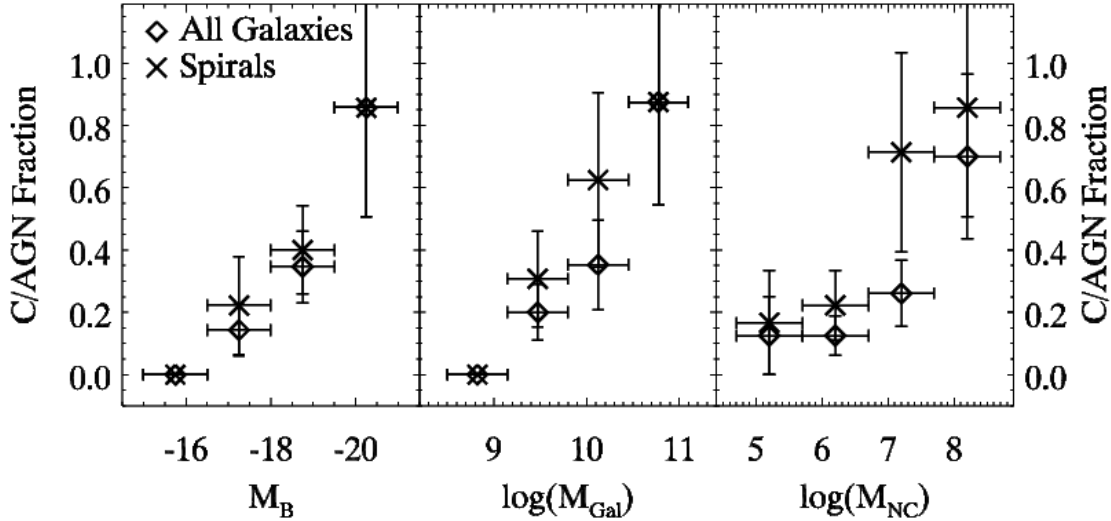
FIG. 6.— Fraction of the 75 galaxies in the spectroscopic sample classified as composite or AGN objects as a function of galaxy B-band absolute magnitude *(left)*, galaxy mass *(center)*, and NC mass *(right)*. In all panels, diamonds indicate the detection rate for all galaxies, while X's include only the spiral galaxies (T>0). The vertical bars show Poisson errors, while the horizontal bars indicate the width of each bin.

$\gtrsim 10\%$ of NCs in our spectroscopic sample host MBHs.

Most of the galaxies with AGN spectra (including the composite objects) are among the brighter and more massive galaxies in our sample. This trend is more clearly seen in Figure 6, which shows the fraction of galaxies in the spectroscopic sample with C/AGN spectra as a function of galaxy B-band absolute magnitude, galaxy mass, and NC mass. A strong correlation is seen in each case, with the highest mass galaxies and NCs having AGN fractions of $\sim 80\%$. This trend of increasing AGN activity with increasing galaxy mass is well documented (e.g., Ho et al. 1997b; Kauffmann et al. 2003; Decarli et al. 2007). The high detection rate of AGN in galaxies with $M_B < -20$ and with galaxy mass of $\sim 10^{11}$ $M_\odot$ is consistent with the findings of these previous surveys. In particular, Decarli et al. (2007) find that almost all Virgo cluster spiral galaxies with dynamical mass $> 10^{11}$ $M_\odot$ have AGN spectra, with little dependence on Hubble type. However, a direct comparison with previous studies is complicated by the strong distance dependence of the detected AGN fraction (Kauffmann et al. 2003) and varying survey depths.

One way of considering whether NCs have any effect on the presence of an AGN is to look at the fraction of AGN as a function of the galaxies' M_{NC}/M_{Gal} (see Figure 2). For galaxies with $M_{NC}/M_{Gal} > 10^{-3}$ the fraction of AGN is very similar (28%) to those with $M_{NC}/M_{Gal} < 10^{-3}$ (25%). This indicates that the trend observed in the right panel of Figure 6 of increasing AGN fraction with increasing NC mass may just reflect the correlation of NC mass with galaxy mass.

Some variation in the AGN fraction is also seen with Hubble type. Ho et al. (1997b) find that transition and AGN spectra are found in $\sim 50\%$ of E and S0 galaxies, 70% of Sa's, 50% of Sb's, and 15% of Sc-Sm's. Unfortunately, direct comparison to our sample is complicated by our inclusion of SDSS data, which differ from the HFS97 data in selection function and sensitivity. Taking just the data from their survey (blue and green points in Figure 5), we classify 1 of 4 E/S0's, 7 of 9 Sa-Sbc's,

and 3 of 10 Sc-Sm's as C/AGN galaxies. Despite the small number of galaxies (and slight differences in the classifications), these detection fractions in our galaxies with NCs are statistically consistent with what Ho et al. (1997b) find for the survey as whole.

The spectroscopic sample does not uniformly cover our full NC galaxy sample. Good SDSS coverage of the Virgo clusters provides spectra for a high fraction of ellipticals ($\sim 75\%$), but the fraction of spirals with spectra is much lower ($\sim 30\%$) and is particularly lacking for the fainter spirals. This lack of spectra hinders our ability to determine the demographic trends of AGN in our sample.

Overall, the demographic evidence suggests that galaxies with NCs have AGN fractions consistent with the population of galaxies as a whole. However, a larger, uniform sample of spectra for galaxies with and without NCs is needed to test this conclusion.

5.2. *The relative mass of nuclear star clusters and massive black holes*

In Ferrarese et al. (2006), the $log(M) - \sigma$ relationship for NCs and MBHs have similar slopes, but the normalizations differ by roughly an order of magnitude, with NCs being more massive at a given bulge velocity dispersion. Similarly, Rossa et al. (2006) find that the normalization of the $M_{NC} - L_{bulge,B}$ relation gives NC masses ~ 3.3 times more massive than the corresponding MBH relation from Marconi & Hunt (2003). Based on a model for the $M_{CMO} - M_{gal}$ relation resulting from feedback of the CMO on the host galaxy, McLaughlin et al. (2006b) suggested this offset may be the result of the reduced efficiency of NC formation feedback relative to feedback from an accreting MBH, thus allowing the NCs to grow larger than an MBH at a given galaxy mass. With the present sample of NCs with AGN activity, we have the opportunity to potentially measure the relative mass of the NCs and MBHs *within the same galaxies*.

For four spiral galaxies from the literature (Milky Way, NGC 4395, NGC 3384, NGC 7457, see §4), we combine direct estimates of the black hole masses and our
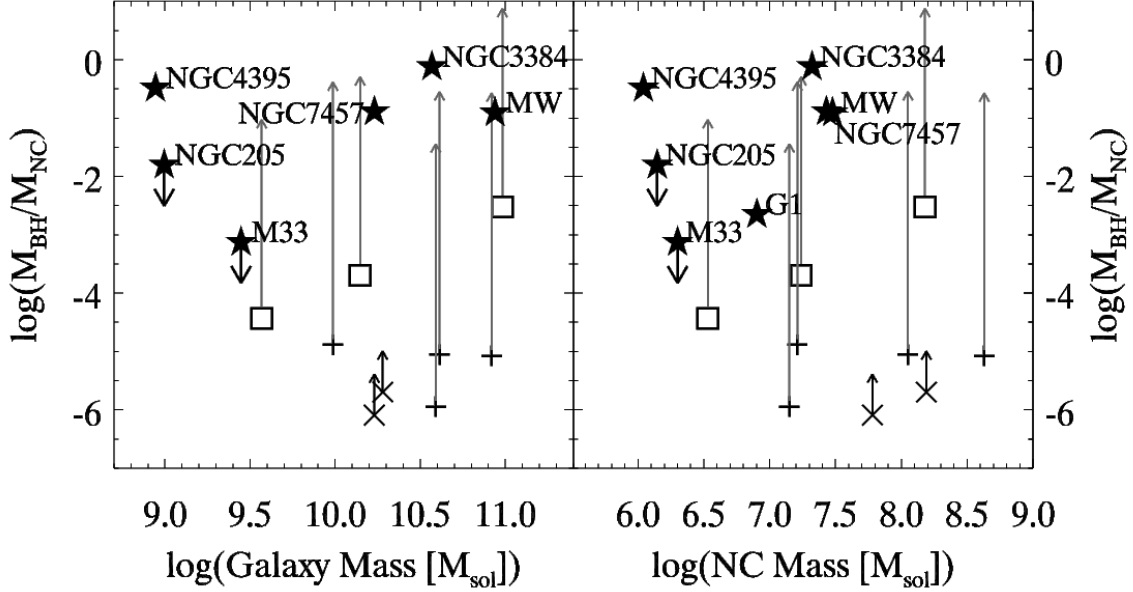
FIG. 7.— Limits on the relative mass of nuclear star clusters and massive black holes as a function of galaxy mass *(left)* and NC mass *(right)*. Stars are galaxies which have measured black hole masses (or upper limits) in the literature (§3.3). The rest of the points represent lower limits based on the bolometric luminosity of their AGN. Different symbols indicate Seyferts (squares), LINERS (crosses), and X-ray sources (X's). For the Seyferts and LINERS, the arrow length indicates the typical L_{bol}/L_{Edd} for each class from Ho (2004).

own estimates of the NC masses (§2.1). Figure 7 shows the galaxy mass vs. M_{BH}/M_{NC} ratios for these objects, which all fall between 0.1 and 1.

We can constrain the M_{BH}/M_{NC} ratio from our sample galaxies by deriving lower limits to the masses of black holes from the bolometric luminosity of the AGN. Both the Hα and [OIII] luminosities are known to be good indicators of the X-ray and bolometric luminosities of low-luminosity AGN of all types (Ho et al. 2001), including sources with significant absorption in the X-ray (Panessa et al. 2006). Because the Hα luminosity suffers more contamination from star-formation, we use [OIII] luminosities to estimate L_X using the Panessa et al. (2006) relation:

$$log(L_X) = 1.22 \, log(L_{[OIII]}) - 7.34 \qquad (1)$$

This yields typical $L_{[OIII]}/L_X \sim 15$ for our sample. We note that in the five cases in our sample where both X-ray data and C/AGN optical spectra are available, their luminosities are consistent with galaxies in the Panessa et al. (2006) sample. In these cases we derive the intrinsic X-ray luminosity based on the observed [OIII] luminosity to correct for any X-ray absorption. Then, for both our optical and X-ray sources, we assume an $L_{bol}/L_X \sim 10$ based on the results of the Ho (1999) for a sample of seven low-luminosity AGN. Note that this is a factor of ~ 3 less than the typically assumed L_{bol}/L_X based on the luminosity function of luminous quasars (Elvis et al. 1994). The derived bolometric luminosities were then divided by the Eddington luminosity for a 1 M$_\odot$ object to obtain a lower limit on the black hole mass. The resulting lower limits on M_{BH}/M_{NC} (actually $(L_{bol}/L_{Edd,\odot})/M_{NC}$) are shown in Figure 7 for the nine strongest AGN candidates in our sample.

The highest lower limit from the sample is observed for NGC 6951, which has $M_{BH}/M_{NC} > 3 \times 10^{-3}$. The mean lower limit on M_{BH}/M_{NC} is 3×10^{-4} for the three Seyfert galaxies (squares), and 6×10^{-6} for the four LINERS

(crosses). For AGN in general (i.e., without respect to the presence of a NC), the mean L_{bol}/L_{Edd} ratios are $\sim 4 \times 10^{-4}$ for Seyferts and $\sim 3 \times 10^{-5}$ for LINERS and composite objects (Ho 2004). If these ratios hold for the AGN in our sample, then our results are consistent with M_{BH}/M_{NC} of near unity. These mean L_{bol}/L_{Edd} ratios are indicated in Figure 7 by the length of the arrows from the Seyfert and LINER data points.

On the other hand, a strong piece of evidence that not all NCs host black holes of similar mass are the non-detections of black holes in Local Group galaxies with nuclear star clusters. In M33, Gebhardt et al. (2001) place an upper limit on the black hole mass of 1500 M$_\odot$. Assuming a mass for the M33 NC of $\sim 2 \times 10^6$ M$_\odot$ (Kormendy & McClure 1993), this non-detection implies an $M_{BH}/M_{NC} \lesssim 10^{-3}$. Similarly, in NGC 205, the upper limit on the black hole mass is 2.2×10^4 M$_\odot$ (Valluri et al. 2005), while the NC mass is 1.4×10^6 M$_\odot$ (De Rijcke et al. 2006), giving $M_{BH}/M_{NC} < 1.6 \times 10^{-2}$.

Finally, the globular cluster G1 in Andromeda, proposed to be the stripped nuclear star cluster of a dwarf galaxy (Meylan et al. 2001), also has an available measurement of M_{BH}/M_{NC}. The globular cluster mass is 8×10^6 M$_\odot$ (Baumgardt et al. 2003) and the black hole mass 1.8×10^4 M$_\odot$ (Gebhardt et al. 2005), giving $M_{BH}/M_{NC} \sim 2 \times 10^{-3}$.

In summary, for four galaxies with measured black hole masses, the ratio of M_{BH}/M_{NC} ranges from 0.1 to 1.0. Candidate AGN in our sample also have luminosities that imply a M_{BH}/M_{NC} of near unity. However, the black hole in the globular cluster G1 and black hole mass upper limits in M33 and NGC 205 show that at least some NCs have much lower M_{BH}/M_{NC} or may not contain a MBH at all. The higher M_{BH}/M_{NC} measurements may result from a bias towards finding high mass black holes in galaxies that have AGN or measurable black hole masses. Overall, the evidence presented here suggests a wide range exists in the relative masses of NCs and

MBHs.

5.3. *Formation Mechanisms*

Based on the scaling relations for central massive objects and the presence of galaxies with both NCs and MBHs, there are two possibilities for the relative formation of central massive objects. Either the formation of MBHs could be directly linked in some way to the formation of NCs, or NCs and MBHs could be produced by processes which scale similarly with galaxy mass, but are otherwise unrelated. We explore the first possibility below.

Because NCs are the dominant objects at the centers of lower mass galaxies (Ferrarese et al. 2006; Wehner & Harris 2006), one natural possibility in hierarchical galaxy formation scenarios is that NCs lead to the formation of MBHs. Formation mechanisms for NCs fall into two classes: those that create NCs from the merging of globular clusters due to dynamical friction (Tremaine et al. 1975; Lotz et al. 2001), and those in which NCs are created *in situ* from gas accretion onto the nucleus due to galaxy merging (Mihos & Hernquist 1994) or from disk gas dynamics (Milosavljević 2004; Bekki et al. 2006). The *in situ* scenario is favored by observations that NCs in spiral galaxies have complicated star formation histories, suggesting frequent episodic star formation (Walcher et al. 2006; Rossa et al. 2006). In addition, Seth et al. (2006) found NCs in late-type spirals that have young stellar disks aligned with the host galaxy disks, indicative of gas accretion onto the nucleus. Côté et al. (2006) also found support for gas accretion in the formation of NCs in elliptical galaxies; their more massive NCs are redder (implying higher metallicity) and more luminous than would be expected if they formed by mergers of globular clusters.

During *in situ* formation, MBH formation could occur through the merging of massive stars at the center of the cluster (see review by Miller & Colbert 2004). For instance, dynamical modelling by Portegies Zwart et al. (2004) of the dense 3.5×10^5 M$_\odot$ cluster MGG 11 in M82 shows that runaway collisions of massive stars leads to the formation of a black hole with mass $\sim 0.2 - 1\%$ of the mass of the cluster. Star formation episodes in NCs could certainly reproduce the high densities and massive star formation required for this mode of MBH formation. However, the MBHs in at least some of the NCs in our sample have masses nearly equal to that of the NC; further accretion onto the MBH would be required to explain these cases. Also, if MBHs were a natural consequence of NC formation, we might expect to see a higher fraction of AGN in galaxies with NCs than for the general galaxy population; this does not appear to be the case (see §5.1). These lines of evidence suggest that if there is a link between formation of NCs and MBHs, the NCs provide at most seed black holes which can then accrete into a more massive black hole.

The lack of NCs in high mass galaxies also provides a clue to the evolution of CMOs. It is possible that during the buildup of more massive galaxies, the NCs could be destroyed (e.g., by black hole merging; Milosavljević & Merritt 2001), leaving behind only an MBH. Alternatively, the presence of an MBH would likely suppress the process of accretion and star formation in the NC due to enhanced feedback, thus preventing

further NC growth.

Theoretical work and simulations are necessary to better understand these processes. Specifically, further simulations of MBH formation in massive clusters are needed that incorporate the episodic gas accretion thought to occur in NCs. Modelling of NCs and MBHs in hierarchical merging scenarios are also essential to explain the demographics of galaxies that host NCs and/or MBHs.

6. CONCLUSIONS AND FUTURE WORK

We have assembled a sample of 176 galaxies known to host nuclear star clusters to study the relationship between nuclear star clusters and massive black holes. We then use optical spectroscopy and radio and X-ray data to look for AGN in this sample. For 75 galaxies with available optical spectra, we classify 7 galaxies as AGN and 11 as composite objects. X-ray catalogs from *Chandra, ROSAT*, and *XMM* provide detections of 22 galaxies in the sample, 4 of which have well-localized sources with X-ray luminosities indicating they are likely AGN. Lastly, we have assembled previously published results for 9 galaxies that indicate they have both NCs and MBHs/AGN; three are included in our sample.

From this work we conclude that galaxies with both NCs and MBHs are relatively common. In addition, by examining the objects in our sample we find that:

1. Galaxies that host both NCs and AGN/MBHs span all Hubble types, have magnitudes as faint as $M_B \sim -16$, and masses as small as 10^9 M$_\odot$. For galaxies in our sample with available spectra, $\gtrsim 10\%$ appear to host both NCs and MBHs.

2. Galaxies with NCs have AGN detection fractions that increase strongly with increasing galaxy and NC mass, consistent with previous studies of the general galaxy population. Variation of the AGN fraction with Hubble type in our sample is also consistent with the full Palomar survey (Ho et al. 1997b). This suggests that nuclear clusters do not play a strong role in promoting or limiting the activity of massive black holes.

3. In four galaxies with NCs and measured black hole masses the ratios of the MBH mass to the NC mass are between 0.1 and 1. The luminosity of the AGN in our sample of galaxies with NCs are also consistent with these mass ratios. However, the nondetection and low masses of MBHs in Local Group NCs suggest a much wider range of MBH-to-NC mass ratios.

4. For galaxies of the same mass, NCs in late-type spiral galaxies are typically an order of magnitude less massive than those in elliptical galaxies. This result will be discussed further in a forthcoming paper.

Although the data presented here provide compelling evidence for a significant overlap between the MBH and NC population, the evidence for the presence of an active MBH in many of the individual objects is quite weak. A number of observations could strengthen this evidence, including high-resolution *Chandra* observations or *Spitzer* mid-IR spectroscopy (e.g., Satyapal et al. 2007).

Furthermore, less than half of the galaxies in our sample have available optical spectroscopy – obtaining spectroscopy for more is desirable and will help fill gaps in parameter space (e.g., the lack of spectra of low-mass early type spiral). Finally, detailed studies of objects with both NCs and MBHs will be required to improve our understanding of the connections between these central massive objects.

REFERENCES

Adelman-McCarthy, J. K. et al. 2007, astro-ph/0707.3413
Baldwin, J. A., Phillips, M. M., & Terlevich, R. 1981, PASP, 93, 5
Baumgardt, H., Makino, J., Hut, P., McMillan, S., & Portegies Zwart, S. 2003, ApJ, 589, L25
Becker, R. H., et al. 1995, ApJ, 450, 559
Becklin, E. E., & Neugebauer, G. 1968, ApJ, 151, 145
Bedin, L. R., Piotto, G., Anderson, J., Cassisi, S., King, I. R., Momany, Y., & Carraro, G. 2004, ApJ, 605, L125
Bekki, K., Couch, W. J., & Shioya, Y. 2006, ApJ, 642, L133
Bell, E. F., McIntosh, D. H., Katz, N., & Weinberg, M. D. 2003, ApJS, 149, 289
Best, P. N. 2004, MNRAS, 351, 70
Böker, T., Laine, S., van der Marel, R. P., Sarzi, M., Rix, H.-W., Ho, L. C., & Shields, J. C. 2002, AJ, 123, 1389
Böker, T., Sarzi, M., McLaughlin, D. E., van der Marel, R. P., Rix, H.-W., Ho, L. C., & Shields, J. C. 2004, AJ, 127, 105
Bruzual, G., & Charlot, S. 2003, MNRAS, 344, 1000
Carollo, C. M., Stiavelli, M., de Zeeuw, P. T., & Mack, J. 1997, AJ, 114, 2366
Carollo, C. M., Stiavelli, M., & Mack, J. 1998, AJ, 116, 68
Carollo, C. M., Stiavelli, M., Seigar, M., de Zeeuw, P. T., & Dejonghe, H. 2002, AJ, 123, 159
Colina, L., Gonzalez Delgado, R., Mas-Hesse, J. M., & Leitherer, C. 2002, ApJ, 579, 545
Condon, J. J., et al. 1998, AJ, 115, 1693
Côté, P. et al. 2006, ApJS, 165, 57
Croft, S., de Vries, W., & Becker, R. H. 2007, astro-ph/0708.0585
De Rijcke, S., Prugniel, P., Simien, F., & Dejonghe, H. 2006, MNRAS, 369, 1321
Decarli, R., Gavazzi, G., Arosio, I., Cortese, L., Boselli, A., Bonfanti, C., & Colpi, M. 2007, astro-ph/0707.0999, 707
Dubus, G., Charles, P. A., & Long, K. S. 2004, A&A, 425, 95
Dudik, R. P., Satyapal, S., Gliozzi, M., & Sambruna, R. M. 2005, ApJ, 620, 113
Efron, B. 1982, The Jackknife, the Bootstrap and other resampling plans (CBMS-NSF Regional Conference Series in Applied Mathematics, Philadelphia: Society for Industrial and Applied Mathematics (SIAM), 1982)
Elvis, M. et al. 1994, ApJS, 95, 1
Fabbiano, G. 2006, ARA&A, 44, 323
Ferrarese, L. et al. 2006, ApJ, 644, L21
Filippenko, A. V., & Ho, L. C. 2003, ApJ, 588, L13
Filippenko, A. V., & Sargent, W. L. W. 1985, ApJS, 57, 503
—. 1989, ApJ, 342, L11
Flesch, E., & Hardcastle, M. J. 2004, A&A, 427, 387
Gebhardt, K. et al. 2001, AJ, 122, 2469
Gebhardt, K., Rich, R. M., & Ho, L. C. 2002, ApJ, 578, L41
—. 2005, ApJ, 634, 1093
Genzel, R., Thatte, N., Krabbe, A., Kroker, H., & Tacconi-Garman, L. E. 1996, ApJ, 472, 153
Ghez, A. M., Salim, S., Hornstein, S. D., Tanner, A., Lu, J. R., Morris, M., Becklin, E. E., & Duchêne, G. 2005, ApJ, 620, 744
Ghosh, K. K., Suleymanov, V., Bikmaev, I., Shimansky, S., & Sakhibullin, N. 2006, MNRAS, 371, 1587
Gonzalez Delgado, R. M., Perez, E., Cid Fernandes, R., & Schmitt, H. 2007, ArXiv e-prints, 710
González-Martín, O., Masegosa, J., Márquez, I., Guerrero, M. A., & Dultzin-Hacyan, D. 2006, A&A, 460, 45
Graham, A. W., & Driver, S. P. 2007, ApJ, 655, 77
Graham, A. W., & Guzmán, R. 2003, AJ, 125, 2936

Greene, J. E., & Ho, L. C. 2007, ApJ, 667, 131
Haberl, F., et al. 2000, A&AS, 142, 41
Ho, L. C. 1999, ApJ, 516, 672
Ho, L. C. et al. 2001, ApJ, 549, L51
Ho, L. C., Filippenko, A. V., & Sargent, W. L. W. 1997a, ApJS, 112, 315
—. 1997b, ApJ, 487, 568
Ho, L. C., Terashima, Y., & Ulvestad, J. S. 2003, ApJ, 589, 783
Ho, L. C. W. 2004, in Coevolution of Black Holes and Galaxies, ed. L. C. Ho, 292–+
Jensen, J. B., Tonry, J. L., Barris, B. J., Thompson, R. I., Liu, M. C., Rieke, M. J., Ajhar, E. A., & Blakeslee, J. P. 2003, ApJ, 583, 712
Jones, D. H. et al. 2004, MNRAS, 355, 747
Kauffmann, G. et al. 2003, MNRAS, 346, 1055
Kennicutt, Jr., R. C. 1998, ApJ, 498, 541
Kewley, L. J., Dopita, M. A., Sutherland, R. S., Heisler, C. A., & Trevena, J. 2001, ApJ, 556, 121
Kewley, L. J., Groves, B., Kauffmann, G., & Heckman, T. 2006, MNRAS, 372, 961
Kormendy, J., & McClure, R. D. 1993, AJ, 105, 1793
Li, Y., Haiman, Z., & Mac Low, M.-M. 2007, ApJ, 663, 61
Lotz, J. M., Telford, R., Ferguson, H. C., Miller, B. W., Stiavelli, M., & Mack, J. 2001, ApJ, 552, 572
Maccarone, T. J., Kundu, A., Zepf, S. E., & Rhode, K. L. 2007, Nature, 445, 183
Maoz, D., Nagar, N. M., Falcke, H., & Wilson, A. S. 2005, ApJ, 625, 699
Marconi, A., & Hunt, L. K. 2003, ApJ, 589, L21
Matthews, L. D. et al. 1999, AJ, 118, 208
McLaughlin, D. E., Anderson, J., Meylan, G., Gebhardt, K., Pryor, C., Minniti, D., & Phinney, S. 2006a, ApJS, 166, 249
McLaughlin, D. E., King, A. R., & Nayakshin, S. 2006b, ApJ, 650, L37
Mei, S. et al. 2007, ApJ, 655, 144
Meylan, G., Sarajedini, A., Jablonka, P., Djorgovski, S. G., Bridges, T., & Rich, R. M. 2001, AJ, 122, 830
Mickaelian, A. M., et al. 2006, A&A, 449, 425
Mihos, J. C., & Hernquist, L. 1994, ApJ, 437, L47
Miller, M. C., & Colbert, E. J. M. 2004, International Journal of Modern Physics D, 13, 1
Milosavljević, M. 2004, ApJ, 605, L13
Milosavljević, M., & Merritt, D. 2001, ApJ, 563, 34
Moran, E. C., Halpern, J. P., & Helfand, D. J. 1996, ApJS, 106, 341
Mukai, K. 1993, Legacy, vol. 3, p.21-31, 3, 21
Nagar, N. M., Falcke, H., & Wilson, A. S. 2005, A&A, 435, 521
Narayan, R., Mahadevan, R., Grindlay, J. E., Popham, R. G., & Gammie, C. 1998, ApJ, 492, 554
Noyola, E., Gebhardt, K., & Bergmann, M. 2006, in Astronomical Society of the Pacific Conference Series, Vol. 352, New Horizons in Astronomy: Frank N. Bash Symposium, ed. S. J. Kannappan, S. Redfield, J. E. Kessler-Silacci, M. Landriau, & N. Drory, 269–+
Osterbrock, D. E. 1989, Astrophysics of gaseous nebulae and active galactic nuclei (University Science Books)
Panessa, F., Bassani, L., Cappi, M., Dadina, M., Barcons, X., Carrera, F. J., Ho, L. C., & Iwasawa, K. 2006, A&A, 455, 173
Panzera, M. R., et al. 2003, A&A, 399, 351

TABLE 1
Optical Spectroscopy for Star-forming Galaxies

Galaxy	log([OIII]/Hβ)	log([NII]/Hα)	log([SII]/Hα)	log([OI]/Hα)	Hα/Hβ[a]	SFR [M$_\odot$/yr]	SDSS Class[b]	HFS97 Class[c]
NGC450	-0.03±0.04	-0.56±0.03	-0.40±0.02	-1.33±0.07	4.1	7.7E-03	HII	$\cdots$
UGC4499	0.11±0.04	-0.89±0.06	-0.40±0.03	-1.34±0.10	3.2	4.6E-04	HII	$\cdots$
NGC2964	-0.55±0.10	-0.31±0.10	-0.58±0.10	-1.77±0.10	5.6	3.5E-01	$\cdots$	HII
NGC3346	-0.56±0.05	-0.45±0.02	-0.50±0.02	-1.53±0.10	3.7	3.4E-03	HII	HII
NGC3913	-0.51±0.08	-0.40±0.03	-0.45±0.03	-1.35±0.12	3.0	1.2E-03	HII	$\cdots$
NGC3949	-0.66±0.10	-0.40±0.10	-0.36±0.10	-1.30±0.30	$\cdots$	$\cdots$	$\cdots$	HII
A1156+52	-0.13±0.06	-0.63±0.04	-0.39±0.03	-1.77±0.30	3.8	2.0E-03	HII	$\cdots$
NGC4144	0.08±0.04	-0.87±0.06	-0.31±0.03	-1.20±0.10	3.2	2.0E-04	HII	HII
NGC4183	-0.08±0.03	-0.62±0.02	-0.45±0.02	-1.58±0.07	5.5	1.1E-02	HII	HII
NGC4244	-0.22±0.11	-0.70±0.09	-0.43±0.06	-1.32±0.24	3.9	1.6E-04	HII	HII
NGC4384	-0.18±0.02	-0.53±0.01	-0.56±0.01	-1.67±0.05	3.2	8.3E-02	HII	$\cdots$
VCC1250	-0.29±0.23	-0.34±0.12	-0.45±0.16	-0.92±0.25	3.9	1.8E-03	HII	$\cdots$
NGC4618	0.14±0.01	-0.71±0.01	-0.54±0.01	-1.62±0.04	3.1	3.7E-03	HII	HII
NGC5585	0.23±0.10	-0.82±0.10	-0.50±0.10	-1.77±0.10	$\cdots$	$\cdots$	$\cdots$	HII
NGC5584	-0.50±0.04	-0.50±0.02	-0.53±0.02	-1.65±0.10	3.5	7.7E-03	HII	$\cdots$
NGC5669	-0.40±0.02	-0.57±0.01	-0.50±0.01	-1.82±0.07	3.5	1.6E-02	HII	HII
NGC5774	-0.41±0.17	-0.41±0.05	-0.22±0.04	-1.14±0.14	4.2	2.2E-03	HII	$\cdots$
NGC6239	0.23±0.01	-0.76±0.01	-0.62±0.01	-1.86±0.03	4.5	6.5E-02	HII	$\cdots$

[a] Galaxies with no data for their Hα/Hβ ratio and SFR are those for which the HFS97 data were not photometric. [b] The classification of HII indicates a star-forming spectra (§3.1). [c] This column gives *our* classification of the HFS97 line ratios.

Paturel, G., Theureau, G., Bottinelli, L., Gouguenheim, L., Coudreau-Durand, N., Hallet, N., & Petit, C. 2003, A&A, 412, 57

Peterson, B. M. et al. 2005, ApJ, 632, 799

Pooley, D., & Rappaport, S. 2006, ApJ, 644, L45

Portegies Zwart, S. F., Baumgardt, H., Hut, P., Makino, J., & McMillan, S. L. W. 2004, Nature, 428, 724

Ptak, A., & Griffiths, R. 2003, in Astronomical Society of the Pacific Conference Series, Vol. 295, Astronomical Data Analysis Software and Systems XII, ed. H. E. Payne, R. I. Jedrzejewski, & R. N. Hook, 465–+

Rasio, F. A. et al. 2006, ArXiv Astrophysics e-prints

Ravindranath, S., Ho, L. C., Peng, C. Y., Filippenko, A. V., & Sargent, W. L. W. 2001, AJ, 122, 653

ROSAT Scientific Team. 2000, VizieR Online Data Catalog, 9028, 0

Rossa, J., van der Marel, R. P., Böker, T., Gerssen, J., Ho, L. C., Rix, H.-W., Shields, J. C., & Walcher, C.-J. 2006, AJ, 132, 1074

Satyapal, S., Vega, D., Heckman, T., O'Halloran, B., & Dudik, R. 2007, ApJ, 663, L9

Scarlata, C. et al. 2004, AJ, 128, 1124

Schödel, R. et al. 2007, A&A, 469, 125

Seth, A. C., Dalcanton, J. J., Hodge, P. W., & Debattista, V. P. 2006, AJ, 132, 2539

Shapley, A., Fabbiano, G., & Eskridge, P. B. 2001, ApJS, 137, 139

Shields, J., Walcher, C. J. M., Boeker, T., Ho, L. C., Rix, H.-W., & van der Marel, R. P. 2008, *submitted*

Shields, J. C. et al. 2007, ApJ, 654, 125

Sivakoff, G. R. et al. 2007, ApJ, 660, 1246

Terashima, Y., & Wilson, A. S. 2003, ApJ, 583, 145

Thim, F., Hoessel, J. G., Saha, A., Claver, J., Dolphin, A., & Tammann, G. A. 2004, AJ, 127, 2322

Tonry, J. L., Dressler, A., Blakeslee, J. P., Ajhar, E. A., Fletcher, A. B., Luppino, G. A., Metzger, M. R., & Moore, C. B. 2001, ApJ, 546, 681

Tremaine, S. et al. 2002, ApJ, 574, 740

Tremaine, S. D., Ostriker, J. P., & Spitzer, L. 1975, ApJ, 196, 407

Tremonti, C. A. et al. 2004, ApJ, 613, 898

Trenti, M. 2006, astro-ph/0612040

Ulvestad, J. S., Greene, J. E., & Ho, L. C. 2007, ApJ, 661, L151

Valluri, M., Ferrarese, L., Merritt, D., & Joseph, C. L. 2005, ApJ, 628, 137

van den Bosch, R., de Zeeuw, T., Gebhardt, K., Noyola, E., & van de Ven, G. 2006, ApJ, 641, 852

van der Marel, R. P. 2004, in Coevolution of Black Holes and Galaxies, ed. L. C. Ho, 37–+

Véron-Cetty, M.-P. et al. 2004, A&A, 414, 487

Voges, W., et al. 1999, A&A, 349, 389

—. 2000, VizieR Online Data Catalog, 9029, 0

Walcher, C. J., Böker, T., Charlot, S., Ho, L. C., Rix, H.-W., Rossa, J., Shields, J. C., & van der Marel, R. P. 2006, ApJ, 649, 692

Walcher, C. J. et al. 2005, ApJ, 618, 237

Wehner, E. H., & Harris, W. E. 2006, ApJ, 644, L17

White, N. E., et al. 1996, VizieR Online Data Catalog, 9012, 0

White, R. L., et al. 2007, ApJ, 654, 99

York, D. G., et al. 2000, AJ, 120, 1579

Yukita, M., Swartz, D. A., Soria, R., & Tennant, A. F. 2007, ApJ, 664, 277

TABLE 2
OPTICAL SPECTROSCOPY FOR COMPOSITE AND AGN GALAXIES

Galaxy	$\log([OIII]/H\beta)$	$\log([NII]/H\alpha)$	$\log([SII]/H\alpha)$	$\log([OI]/H\alpha)$	$H\alpha/H\beta$ [a]	$L_{[OIII]}/L_\odot$	SDSS Class[b]	HFS97 Class[c]
NGC428	-0.12±0.10	-0.25±0.10	0.12±0.10	<-0.72	···	···	···	C/L2
NGC1042	-0.01±0.02	-0.26±0.01	-0.45±0.02	-1.20±0.04	3.6	6.7E+04	C	···
NGC3177	-0.43±0.03	-0.20±0.01	-0.58±0.02	-1.40±0.05	5.6	3.7E+05	C	···
NGC3259	0.72±0.04	-0.13±0.03	-0.41±0.04	-0.94±0.06	4.9	5.6E+05	AGN/S2	···
NGC3423	-0.38±0.10	-0.31±0.05	-0.38±0.05	-1.15±0.14	3.4	3.4E+03	C	C
NGC3928	-0.25±0.02	-0.31±0.01	-0.51±0.01	-1.47±0.04	3.2	1.3E+05	C	···
NGC4206	-0.13±0.15	-0.31±0.09	-0.26±0.08	-1.17±0.30	3.9	2.0E+03	C	···
NGC4411B	0.39±0.37	-0.19±0.10	-0.27±0.12	-0.91±0.25	7.2	3.7E+04	AGN/S2	···
NGC4517	0.09±0.17	-0.29±0.10	-0.25±0.10	-1.27±0.10	7.7	5.2E+04	···	C/L2
VCC1619	0.27±0.10	-0.26±0.10	0.05±0.10	-0.77±0.10	···	···	···	C/L2
NGC4625	-0.35±0.10	-0.31±0.05	-0.33±0.05	-1.00±0.10	3.2	2.1E+03	C	···
NGC4750	0.24±0.10	0.46±0.10	0.30±0.10	-0.22±0.10	3.3	2.0E+05	···	AGN/L1.9
NGC5377	0.30±0.17	0.33±0.10	0.22±0.10	-0.60±0.10	4.6	5.8E+05	···	AGN/L2
NGC5678	-0.17±0.08	-0.22±0.03	-0.48±0.05	-1.20±0.12	7.0	3.7E+05	C	C
NGC5806	-0.05±0.07	-0.15±0.05	-0.38±0.06	-1.07±0.14	4.1	8.4E+04	C	C
NGC5879	0.08±0.06	-0.05±0.05	-0.05±0.05	-0.68±0.08	3.6	2.6E+04	AGN/L2	AGN
NGC6384	0.18±0.17	0.24±0.10	0.03±0.10	<-0.82	3.1	6.8E+03	···	AGN/L2
NGC6951	0.82±0.10	0.39±0.10	-0.04±0.10	-0.64±0.10	16.7	3.0E+07	···	AGN/S2

[a] Galaxies with no data for their $H\alpha/H\beta$ ratio and [OIII] luminosity are those for which the HFS97 data were not photometric. [b] Classes are defined in §3.1, "C"=composite, "L"=LINER and "S"=Seyfert. [c] This column gives *our* classification of the HFS97 line ratios.

TABLE 3
RADIO DATA FOR THE 13 GALAXIES WITH FIRST MATCHES.

Galaxy	Optical Class	Separation NC ($''$)	Integrated Flux (mJy)	RMS ($''$)	Major Axis ($''$)	Minor Axis ($''$)	$L_{1.4GHz}$ (W Hz^{-1})
NGC 2964	HII	0.2	28.38	0.14	6.98	4.99	1.5×10^{21}
NGC 3177	C	1.0	26.21	0.24	9.47	7.56	1.3×10^{21}
NGC 3277	···	0.6	3.29	0.14	7.40	6.77	1.9×10^{20}
NGC 3928	C	0.7	8.55	0.14	10.11	8.99	2.6×10^{20}
NGC 3949	HII	24.9	21.08	0.14	23.21	17.68	5.4×10^{20}
NGC 4030	···	10.0	34.26	0.16	41.07	26.28	1.8×10^{21}
NGC 4144	HII	14.9	1.56	0.14	3.82	0.00	9.8×10^{18}
VCC 437	···	25.9	4.94	0.13	9.19	8.38	1.6×10^{20}
NGC 4384	HII	3.3	12.52	0.15	14.39	10.39	2.3×10^{21}
NGC 4701	···	3.6	5.93	0.15	18.66	8.88	8.8×10^{19}
NGC 5377	AGN/L2	1.4	3.26	0.14	6.94	6.61	3.8×10^{20}
NGC 5678[a]	C	7.2	68.39	0.14	44.03	32.26	6.6×10^{21}
NGC 6239[a]	HII	0.8	4.11	0.17	11.96	5.43	1.4×10^{20}

NOTE. — All of these galaxies were also detected by NVSS.
[a] Flagged as a possible sidelobe of a nearby bright source. NGC 5377 has two other fainter FIRST sources within 20$''$ of the NC position; NGC 6239 has no other FIRST sources within 60$''$. It is unclear why these radio sources are flagged.

TABLE 4
X-RAY DATA FOR THE 22 GALAXIES WITH *Chandra*, *ROSAT*, OR *XMM* MATCHES.

Galaxy	Optical[a] Class	X-ray Source Name	Separation NC ($''$)	Extent ($''$)	L_X[b], $2-10$ keV (erg s^{-1})
Chandra					
VCC 751	$\cdots$	X122448.46+181141.8	1.3	2.0×2.0	1.58×10^{38}
VCC 828	ABS	X122541.63+124837.3	1.3	5.0×5.0	3.25×10^{38}
VCC 1192	$\cdots$	X122930.21+075934.6	0.8	0.7×0.6	2.37×10^{38}
NGC 4750	AGN/L1.9	X125007.34+725228.8	1.0	0.4×0.4	1.05×10^{40}
NGC 5678	C	X143205.54+575517.2	0.5	0.7×0.3	6.67×10^{38}
NGC 5774	HII	X145342.77+033503.2	4.9	0.7×0.6	1.17×10^{38}
NGC 5879	AGN/L2	X150946.72+570000.2	1.0	1.0×0.5	2.51×10^{38}
ROSAT					
NGC 600	$\cdots$	2RXP J013305.7−071835	9.8	0	8.10×10^{39}
NGC 1385[c]	$\cdots$	1BMW 033728.0−243003	4.1	14	1.13×10^{40}
NGC 2566[d]	$\cdots$	1RXS J081847.0−252922	40.7	0	2.69×10^{40}
NGC 3259	AGN/S2	RX J103234+65024	9.4	0	1.27×10^{40}
NGC 3445	$\cdots$	1WGA J1054.5+5659	9.4	$\cdots$	2.66×10^{39}
NGC 4030	$\cdots$	RX J120023−01055	10.8	9	1.47×10^{40}
NGC 4540[d]	$\cdots$	1RXS J123456.0+153314	74.1	0	7.60×10^{40}
NGC 6000[c]	$\cdots$	1RXH J154949.7−292310	3.6	0	5.83×10^{40}
XMM					
NGC 1493	$\cdots$	2XMM J035727.3−461239	4.5	< 6	3.51×10^{38}
VCC 1250	HII	2XMM J122959.1+122052	3.0	< 6	3.23×10^{38}
VCC 1283	ABS	2XMM J123018.3+133440	0.7	< 6	2.82×10^{38}
VCC 1355	$\cdots$	2XMM J123120.2+140656	1.8	< 6	4.37×10^{38}
NGC 4517	C	2XMM J123245.4+000655	1.8	< 6	7.25×10^{38}
NGC 6951	AGN/S2	2XMM J203714.0+660619	0.5	< 6	5.39×10^{39}
NGC 7418	$\cdots$	2XMM J225636.0−370145	1.5	< 6	6.37×10^{39}

[a] Classes identified in §3.1; "ABS"=absorption spectrum. [b] Assuming $\Gamma = 1.8$. [c] *ROSAT*/HRI detection. [d] Tentatively associated with X-ray source.

TABLE 5
GALAXIES WITH NUCLEAR STAR CLUSTERS SAMPLE

Galaxy	Type	T	D [Mpc]	M_B	$\log(M_{gal}/M_\odot)$	Source[a]	NC r_{eff}[b]	$\log(M_{NC}/M_\odot)$	Spectra[c]
NGC275	SBc	6.0	24.0	-19.1	$\cdots$	B02	0.05	6.3	None
NGC289	SBbc	3.9	27.4	-20.5	10.9	C02	0.13	7.9	None
NGC300	Scd	6.9	1.9	-17.6	9.3	B02	0.13	6.0	None
NGC337a	SABd	7.9	14.3	-17.9	9.4	B02	0.06	5.3	None
NGC406	Sc	4.9	17.5	-18.2	9.7	C02	0.10	5.8	None
NGC428	SABm	8.6	15.9	-19.1	9.8	B02	0.05	6.5	HFS97
NGC450	SABc	5.9	24.4	-19.2	9.7	B02	0.11	6.1	SDSS
NGC600	Scd	6.9	25.1	-19.0	9.9	B02	0.06	6.2	None
NGC853	Sm	8.7	21.0	-15.9	9.6	B02	0.05	6.1	None
NGC986	Sab	2.3	24.9	-20.3	10.9	C02	0.11	7.9	None
NGC1042	SABc	6.0	18.0	-19.6	10.0	B02	0.05	6.5	SDSS
NGC1325	SBbc	4.0	20.1	-19.3	10.3	C98	0.09	7.1	None
ESO548-G10	Scd	6.8	16.5	-17.7	9.4	C97	0.07	6.9	None
ESO358-5	SABm	8.8	20.0	-16.7	9.4	B02	0.05	5.9	None
NGC1345	Sc	5.1	19.5	-17.1	9.2	C02	0.05	6.1	None
ESO548-G29	SABb	3.4	16.2	-16.7	$\cdots$	C02	0.04	5.9	None
ESO418-8	SABd	7.9	14.1	-16.7	9.4	B02	0.05	5.5	None
NGC1385	Sc	5.9	18.6	-19.9	10.3	C98	0.04	6.4	None
ESO482-G17	Sab	2.2	18.5	-16.1	10.0	C97	0.15	6.7	None
ESO549-G18	SABc	5.0	20.0	-17.9	9.9	C02	0.17	6.2	None
NGC1483	SBbc	4.0	12.6	-17.3	9.1	C02	0.03	5.3	None
NGC1493	SBc	6.0	11.3	-18.4	9.6	B02	0.06	6.4	None
ESO202-41	SBm	9.0	19.8	-16.3	9.3	B02	0.06	5.0	None
NGC1688	SBc	6.2	13.4	-18.5	9.5	C02	0.06	6.3	None
NGC1892	Sc	5.8	15.2	-18.1	9.6	C02	0.05	6.7	None
NGC2082	SBb	3.2	15.3	-18.2	9.8	C02	0.06	6.3	None
NGC2104	SBm	8.9	12.8	-17.3	9.1	C97	0.13	5.7	None
ESO205-G7	SBb	3.0	24.7	-16.6	9.7	C02	0.12	7.6	None
NGC2139	Sc	5.9	23.6	-19.9	10.1	B02	0.07	5.9	None
UGC3574	Sc	5.9	23.3	-17.8	$\cdots$	B02	0.06	6.1	None
NGC2397	SBb	3.1	15.1	-18.2	10.1	C97	0.27	8.5	None
UGC3826	SABc	6.5	27.8	-17.6	$\cdots$	B02	0.07	5.6	None
NGC2566	Sb	2.8	21.0	-19.7	10.7	C02	0.11	8.7	None
NGC2552	SABm	9.0	10.0	-17.3	9.0	B02	0.05	5.8	SDSS
UGC4499	Sd	7.9	12.6	-16.2	8.7	B02	0.07	4.9	SDSS
NGC2758	SBbc	3.9	26.1	-17.9	10.0	C02	0.07	6.5	None
NGC2763	SBc	5.6	25.4	-19.4	10.1	B02	0.07	5.9	None
NGC2805	SABc	6.9	28.2	-20.5	10.0	B02	0.06	6.7	None
UGC4988	Sm	8.7	24.3	-16.6	9.1	B02	0.05	5.8	SDSS
ESO498-G5	SABb	4.3	32.4	-18.5	10.1	C02	0.05	7.3	None
UGC5015	SABd	7.7	25.4	-16.6	9.1	B02	0.06	5.9	SDSS
IRAS09312-3248	Sc	6.0	10.6	-17.4	9.6	S06	*	5.0	None
NGC2964	Sbc	4.1	20.6	-19.5	10.5	C02	0.14	7.8	HFS97
NGC3045	Sb	3.0	30.5	-18.5	9.9	C98	0.08	6.8	None
ESO499-G37	SABc	6.2	11.5	-16.8	8.4	C02	0.28	5.8	None
NGC3177	Sb	3.0	20.1	-18.5	10.1	C98	0.09	8.1	SDSS
NGC3259	SABb	3.6	27.5	-19.3	10.1	C02	0.11	7.2	SDSS
NGC3277	Sab	1.8	22.0	-19.2	10.4	C02	0.15	8.3	None
NGC3346	SBc	6.0	18.9	-19.0	$\cdots$	B02	0.04	6.1	S&H
NGC3423	Sc	6.0	14.7	-19.2	9.9	B02	0.06	6.5	S&H
NGC3455	SABb	3.1	16.9	-16.8	9.5	C02	0.04	6.8	None
NGC3445	SABm	8.9	32.1	-19.6	9.9	B02	0.05	6.7	None
NGC3501	Sc	5.9	17.4	-17.7	$\cdots$	S06	*	5.9	None
NGC3782	Scd	6.6	13.6	-17.6	$\cdots$	B02	0.05	5.4	None
NGC3885	S0-a	0.2	24.1	-19.0	9.9	C97	0.22	8.4	None
NGC3906	SBcd	6.8	16.9	-17.6	9.3	B02	0.06	5.4	None
NGC3913	Scd	6.6	17.1	-17.8	9.4	B02	0.25	5.3	SDSS
NGC3928	E	-4.5	15.8	-17.8	9.7	C02	0.10	7.4	SDSS
NGC3949	Sbc	4.0	14.6	-19.5	9.9	C02	0.05	6.9	HFS97
ESO572-G22	SBcd	6.7	26.3	-17.1	9.6	C02	0.04	6.2	None
ESO504-30	SBd	7.7	24.0	-17.0	8.9	B02	0.06	5.9	None
UGC6931	SBm	9.0	20.6	-16.0	$\cdots$	B02	0.05	5.3	None
A1156+52	SBc	5.8	18.8	-18.1	9.4	B02	0.05	5.7	SDSS
NGC4027	SBd	7.8	22.8	-20.2	10.5	B02	0.07	5.9	None
NGC4030	Sbc	4.0	21.1	-20.4	10.9	C98	0.09	8.0	None
NGC4144	SABc	6.0	7.2	-17.2	9.0	S06	0.05	4.8	S&H
VCC33	E?	-2.4	16.5	-16.3	$\cdots$	C06	0.03	5.7	SDSS
NGC4183	Sc	5.9	16.2	-18.2	9.6	S06	*	5.9	S&H
VCC140	S0-a	0.3	16.5	-16.7	$\cdots$	C06	0.03	5.7	SDSS
NGC4204	SBd	7.9	13.9	-16.9	$\cdots$	B02	0.07	5.4	None
NGC4206	Sbc	4.0	11.3	-17.4	9.5	S06	0.18	6.8	SDSS
VCC200	E	-4.1	16.5	-16.3	9.0	C06	0.05	5.4	SDSS
VCC230	E?	-2.5	16.5	-15.8	8.8	C06	0.04	6.5	SDSS
NGC4244	Sc	6.1	4.3	-17.7	9.3	S06	0.16	6.5	S&H
VCC437	S0	-2.5	16.5	-16.5	9.3	C06	0.09	6.6	None

TABLE 5 — *Continued*

Galaxy	Type	T	D [Mpc]	M_B	$\log(M_{gal}/M_\odot)$	Source[a]	NC r_{eff}[b]	$\log(M_{NC}/M_\odot)$	Spectra[c]
NGC4299	SABd	8.3	16.8	-18.4	9.3	B02	0.05	6.0	None
VCC538	E-S0	-3.3	16.5	-15.6	8.8	C06	0.03	6.2	None
VCC543	S0-a	-1.0	16.5	-16.3	$\cdots$	C06	0.16	5.8	SDSS
VCC698	S0	-2.0	16.5	-17.5	9.8	C06	0.04	6.8	SDSS
VCC751	S0-a	0.1	16.5	-15.7	9.2	C06	0.05	6.1	None
NGC4384	Sa	1.0	39.3	-19.4	10.1	C02	0.06	6.3	SDSS
VCC784	E-S0	-2.8	16.5	-18.4	10.1	C06	0.16	7.7	HFS97
VCC828	E	-4.8	16.5	-18.1	10.0	C06	0.21	7.5	SDSS
VCC856	E-S0	-2.9	16.5	-16.6	9.3	C06	0.16	7.1	SDSS
NGC4416	Sc	5.9	20.8	-18.5	$\cdots$	B02	0.22	4.9	None
NGC4411B	SABc	6.1	19.1	-18.4	9.6	B02	0.06	6.5	SDSS
VCC1075	E?	-2.7	16.5	-16.0	8.9	C06	0.04	6.1	SDSS
VCC1087	E	-4.1	16.5	-16.7	9.4	C06	0.03	6.7	SDSS
VCC1125	S0	-1.8	16.5	-18.2	10.0	C06	0.06	6.4	SDSS
VCC1146	E	-4.8	16.5	-18.2	10.0	C06	0.78	8.7	None
VCC1185	E	-4.2	16.5	-15.6	8.8	C06	0.06	6.2	SDSS
VCC1192	E	-4.8	16.5	-16.2	9.4	C06	0.12	7.1	None
VCC1199	E	-4.1	16.5	-15.5	8.9	C06	0.08	6.9	None
VCC1242	S0	-2.0	16.5	-18.6	10.2	C06	0.04	7.1	None
VCC1250	E-S0	-3.0	16.5	-17.9	9.9	C06	0.03	7.0	SDSS
VCC1261	E	-4.8	16.5	-17.4	9.5	C06	0.04	7.0	SDSS
VCC1283	S0	-1.8	16.5	-17.6	9.9	C06	0.05	6.7	SDSS
NGC4487	Sc	5.9	14.7	-19.0	9.8	B02	0.05	6.6	None
VCC1355	E	-4.8	16.5	-16.5	$\cdots$	C06	0.04	6.2	None
NGC4496A	SBd	7.5	15.0	-18.8	9.7	B02	0.05	5.7	None
VCC1407	E	-4.1	16.5	-16.0	9.0	C06	0.14	6.4	SDSS
VCC1422	E	-4.8	16.5	-17.1	9.4	C06	0.04	6.7	SDSS
VCC1431	E	-4.0	16.5	-16.7	9.4	C06	0.24	6.8	SDSS
VCC1440	E	-4.4	16.5	-16.1	9.2	C06	0.06	6.9	SDSS
NGC4517	Sc	6.0	16.5	-20.0	10.6	S06	0.04	6.8	HFS97
VCC1488	E-S0	-2.9	16.5	-16.2	8.9	C06	0.03	5.0	SDSS
VCC1489	E	-5.0	16.5	-15.2	8.6	C06	0.05	5.6	SDSS
VCC1528	E	-4.2	16.5	-16.5	9.4	C06	*	5.7	SDSS
VCC1539	E	-5.0	16.5	-15.6	8.6	C06	0.23	6.3	SDSS
VCC1545	E	-3.6	16.5	-16.3	8.9	C06	0.05	5.9	SDSS
NGC4540	SABc	6.1	19.9	-19.0	$\cdots$	B02	0.07	6.2	None
VCC1619	S0	-2.0	16.5	-18.6	10.2	C06	0.32	8.1	HFS97
VCC1627	E-S0	-3.3	16.5	-15.6	9.2	C06	0.20	7.4	SDSS
VCC1630	E	-4.8	16.5	-18.2	10.2	C06	0.50	8.0	None
VCC1661	E	-5.0	16.5	-15.3	8.6	C06	0.08	6.5	SDSS
VCC1695	S0-a	-0.8	16.5	-16.4	9.3	C06	*	5.8	SDSS
VCC1720	S0	-2.0	16.5	-18.7	10.3	C06	0.09	7.6	HFS97
VCC1826	E	-3.6	16.5	-16.0	8.8	C06	*	6.7	SDSS
VCC1828	Sc	5.4	16.5	-15.9	8.8	C06	0.06	6.0	SDSS
VCC1861	E	-4.8	16.5	-16.6	9.3	C06	0.14	6.6	SDSS
VCC1871	S0	-2.2	16.5	-17.2	$\cdots$	C06	0.12	7.3	SDSS
NGC4618	SBm	8.6	10.7	-18.8	9.6	B02	0.10	6.0	S&H
VCC1883	S0	-2.0	16.5	-19.0	10.4	C06	*	7.2	HFS97
VCC1886	E	-5.0	16.5	-16.1	$\cdots$	C06	0.04	5.8	SDSS
VCC1895	E	-3.5	16.5	-16.1	9.0	C06	*	5.1	None
NGC4625	SABm	8.8	11.7	-17.3	9.4	B02	0.10	5.6	SDSS
VCC1910	E	-4.8	16.5	-16.8	9.5	C06	0.04	6.8	SDSS
VCC1913	S0-a	-1.5	16.5	-17.8	9.9	C06	0.60	7.9	None
VCC2019	E	-3.5	16.5	-16.4	9.2	C06	0.04	6.6	None
VCC2048	E	-4.7	16.5	-17.2	9.6	C06	0.04	6.1	None
VCC2050	E	-5.0	16.5	-15.8	$\cdots$	C06	0.07	5.6	SDSS
NGC4701	Sc	5.8	11.1	-17.4	9.3	B02	0.04	6.5	None
NGC4750	Sab	2.4	27.2	-20.3	10.6	C02	0.14	8.1	HFS97
NGC4775	Scd	6.9	22.5	-20.2	$\cdots$	B02	0.06	7.6	None
NGC4806	Sc	4.9	32.7	-19.0	$\cdots$	C02	0.05	7.0	None
NGC4980	Sa	1.1	19.1	-17.8	9.4	C02	0.05	6.4	None
NGC5023	Sc	6.0	5.4	-15.9	8.7	S06	0.32	5.3	None
ESO508-G34	SABd	8.3	26.2	-17.2	8.8	C98	0.06	6.4	None
NGC5068	Sc	6.0	8.7	-19.0	10.0	B02	0.11	6.2	None
NGC5188	Sb	3.0	32.7	-19.6	10.7	C02	0.20	8.1	None
UGC8516	Sc	5.9	16.7	-17.3	9.3	B02	0.09	5.8	None
NGC5377	Sa	1.1	31.0	-20.3	10.9	C02	0.18	8.6	HFS97
IC4390	SABb	4.3	27.8	-18.3	$\cdots$	C02	0.17	8.1	None
NGC5585	SABc	6.9	10.5	-18.7	9.4	B02	0.06	5.8	HFS97
NGC5584	SABc	5.9	24.3	-19.4	10.1	B02	0.08	5.1	SDSS
NGC5678	SABb	3.3	28.3	-20.3	10.8	C02	0.18	8.1	S&H
NGC5669	SABc	6.0	21.2	-19.0	$\cdots$	B02	0.05	6.5	S&H
NGC5774	SABc	6.9	23.7	-18.8	9.8	B02	0.12	5.5	SDSS
NGC5789	SBd	7.8	28.7	-18.3	$\cdots$	B02	0.07	5.5	None
NGC5806	Sb	3.1	21.4	-19.3	10.5	C02	0.21	8.1	S&H
NGC5879	Sbc	3.5	15.0	-18.8	10.0	C97	0.17	7.2	S&H

TABLE 5 — *Continued*

Galaxy	Type	T	D [Mpc]	M_B	$\log(M_{gal}/M_\odot)$	Source[a]	NC r_{eff}[b]	$\log(M_{NC}/M_\odot)$	Spectra[c]
NGC5964	SBcd	6.9	22.2	-18.4	9.8	B02	0.06	6.4	None
NGC6000	SBbc	3.9	35.2	-19.6	10.3	C02	0.17	8.2	None
NGC6239	SBb	3.2	16.9	-18.2	9.6	C02	*	6.7	SDSS
ESO138-10	Sd	7.8	13.5	-18.9	10.3	B02	0.09	7.0	None
NGC6384	SABb	3.6	16.7	-19.5	10.6	C02	0.14	7.2	HFS97
NGC6509	SABc	6.6	27.5	-19.0	$\cdots$	B02	0.04	6.4	None
NGC6951	SABb	3.9	24.8	-20.0	11.0	C02	0.18	8.2	HFS97
IC5052	SBcd	7.1	6.0	-17.2	9.1	S06	0.10	5.9	None
ESO404-G3	SBbc	4.0	31.9	-18.3	9.7	C02	0.03	6.4	None
NGC7162	Sc	4.8	30.3	-19.1	10.0	C02	0.11	6.8	None
NGC7188	SBbc	3.6	24.1	-17.8	9.5	C02	0.06	6.9	None
NGC7259	Sb	2.8	22.8	-17.8	$\cdots$	C02	0.06	6.9	None
IC5256	SBd	7.7	9.9	-15.2	$\cdots$	C98	*	5.1	None
NGC7418	Sc	5.8	18.3	-19.6	10.2	B02	0.06	7.8	None
NGC7421	Sbc	3.8	23.7	-19.2	10.2	C02	0.11	6.9	None
NGC7424	Sc	5.9	10.8	-19.1	9.6	B02	0.10	6.1	None
IC5271	Sb	3.1	23.9	-19.5	10.6	C02	0.11	7.9	None
ESO290-39	SBm	8.9	19.1	-16.2	$\cdots$	B02	0.07	4.9	None
NGC7513	SBb	3.2	20.4	-18.9	10.1	C02	0.06	7.0	None
NGC7690	Sb	2.8	18.2	-18.3	9.8	C02	0.17	8.0	None
NGC7689	SABc	6.0	24.8	-19.8	10.3	B02	0.08	6.9	None
ESO240-G12	Sb	3.1	23.0	-17.3	9.3	C02	0.03	6.0	None
UGC12732	SABm	8.7	12.3	-16.3	$\cdots$	B02	0.07	5.8	None
ESO241-6	SBm	8.9	17.3	-16.7	$\cdots$	B02	0.06	5.3	None
NGC7793	Scd	7.4	3.9	-18.3	9.6	B02	0.10	6.9	None

[a] Sources are "B02"=Böker et al. (2002), "C06"=Côté et al. (2006), "C02"=Carollo et al. (2002), "C99"=Carollo et al. (1998), "C97"=Carollo et al. (1997), "S06"=Seth et al. (2006). [b] NCs with sizes of '*' were unresolved by HST observations and thus have $r_{eff} \lesssim 0.03''$. [c] S&H refers to spectra present in both SDSS and HFS97.